MLM-2414

MLM-2414

Mound Laboratory Activities in Chemical and Physical Research: July-December 1976

May 4, 1977

MOUND LABORATORY
Miamisburg, Ohio
operated by
MONSANTO RESEARCH CORPORATION
a subsidiary of Monsanto Company
for the
UNITED STATES ENERGY RESEARCH AND DEVELOPMENT ADMINISTRATION

U. S. Government Contract No. EY-76-C-04-0053

Monsanto

DISCLAIMER

NOTICE

MLM-2414
TID-4500
Distribution Categories
UC-4 and UC-22

Mound Laboratory Activities in Chemical and Physical Research: July-December 1976

Issued: May 4, 1977

PRINTED IN THE UNITED STATES OF AMERICA

Available from
National Technical Information Service
U. S. Department of Commerce
5285 Port Royal Road
Springfield, Virginia 22161
Price: Printed Copy $4.00; Microfiche $3.00

MONSANTO RESEARCH CORPORATION
A Subsidiary of Monsanto Company

MOUND LABORATORY
Miamisburg, Ohio 45342
operated for

UNITED STATES ENERGY RESEARCH AND DEVELOPMENT ADMINISTRATION

U. S. Government Contract No. EY-76-C-04-0053

Foreword

The present report, Mound Laboratory Activities in Chemical and Physical Research, issued semiannually, replaces the former semiannual report entitled Mound Laboratory Activities for the Division of Physical Research. Under the sponsorship of the ERDA Division of Physical Research, Mound Laboratory is responsible for producing materials for use in the physical sciences to further the progress of science and technology in the public interest. Additional research activities of related interest under the sponsorship of the Division of Military Application are also reported here.

This report is submitted by W. T. Cave, Director of Nuclear Operations, and R. E. Vallee, Manager of Technology Applications and Development, from contributions prepared by W. M. Rutherford, Science Fellow (Thermal Diffusion); W. L. Taylor, Science Fellow (Gas Dynamics and Cryogenics); G. L. Silver, Senior Research Specialist (Separation Chemistry); R. C. Bowman, Leader, Metal Hydride Research, and from members of the Isotope Separation Section: R. A. Schwind, Isotope Separation Manager; E. Michaels, Leader, Isotope Separations Development; W. J. Roos, Leader, Stable Isotopes Production; B. E. Jepson, Leader, Metal Isotope Separation; R. M. Watrous, Leader, Radioisotopes Separation; and V. L. Avona, Leader, Stable Isotope Sales.

These reports are not intended to constitute publication in any sense of the word. Final results will either be submitted for publication in regular professional journals or be published in the form of MLM topical reports.

P. A. Semple, Editor

Table of Contents

Page

ISOTOPE SEPARATION

ARGON 6

Production of 7% argon-38 and 99.5% argon-36 continued during this period.

CARBON. 6

During this period, 99% carbon-13 methane, 97% carbon-13 dioxide, and 97% elemental carbon-13 were produced.

Results of preliminary experiments conducted with the first batch of carbon-12 methane, highly depleted in carbon-13, indicate that the carbon-13 concentration is less than 10 ppm, thereby meeting the prescribed product specifications.

Enrichment of a special batch of carbon-13 methane to a carbon-13 concentration greater than 99.9% has been completed.

HELIUM. 6

A total of approximately 4400 liters of helium, grading 99.9% helium-3, was produced.

KRYPTON 6

A nine-column thermal diffusion cascade and a 19-column cascade have continued producing 99% krypton-86.

The 10-column cascade has produced a batch of 90% krypton-82 and a batch of 90% krypton-80.

Radiometric Krypton Three batches of krypton, highly depleted in krypton-85, were shipped from Mound Laboratory. This material, along with one batch shipped earlier, fulfills the requirements of the Radiometric Krypton Program.

NEON 6

A six-column thermal diffusion cascade produced approximately 0.5 STP liter of 90% neon-21.

Upgrading of batches of neon-20 and neon-22, which are slightly below product specifications, has continued.

OXYGEN. 6

An electrolysis system for producing oxygen-16 gas was constructed and appears to operate satisfactorily on a pilot scale.

SULFUR. 6

Checkout of the sulfur isotopes chemical exchange system has been completed. Start-up has been delayed due to lack of manpower.

XENON 7

During this period, three thermal diffusion systems produced the following quantities of product: 1.0 STP liter of 2% xenon-126, 2.5 STP liters of 5% xenon-124, 0.65 STP liter of 40% xenon-124, 11 STP liters of 80% xenon-136, and a batch of 50% xenon-134.

Page

LOW TEMPERATURE RESEARCH

VAPOR PRESSURE STUDIES 7

Vapor pressure ratios have been measured for D_2 mixtures with concentrations of para molecules up to 82%. Unexplained time dependent effects have been observed. Rapid ortho-para conversion must be reduced to obtain reliable data.

METAL HYDRIDE RESEARCH

PULSE NMR STUDIES 11

Studies of $TiFeH_x$ The nuclear relaxation times T_2^*, T_2', and T_1 have been measured for protons in a γ-phase $Ti_{1.04}Fe_{0.96}H_{2.0}$ sample provided by the National Bureau of Standards. These measurements confirm an earlier observation that strong nuclear spin-conduction electron interactions occur in γ-phase $TiFeH_x$, yielding a Korringa constant $C_K = 5.4$ sK. The hydrogen mobility in γ-phase $TiFeH_x$ does not influence either T_1 or T_2'; hence, the hydrogen diffusion constant at room temperature is $<10^{-11}$ cm^2/s.

Low Temperature Ordering in VH_x The ordering of hydrogen atoms during low temperature phase transformations of β-phase VH_x is being investigated. Proton-proton interactions have been measured below 200 K using a $\pi/2-\tau-\pi$ spin echo pulse sequence and then compared with dipolar second moments calculated for (1) proposed V_4H_2, V_6H_4, V_8H_6, and V_4H_4 superstructures and (2) random occupants of lattice sites. The best agreement between theory and experiment has been obtained with a model developed in this study in which the H-H separation is maximized.

ELECTRON PARAMAGNETIC RESONANCE STUDIES OF TRANSITION METAL IONS IN METAL HYDRIDES. 16

Analysis of the electron paramagnetic resonance (EPR) spectra for Species B in LiH and LiD single crystals indicates that it arises from an axial rhodium complex with an unpaired electron in a $4d_{x^2-y^2}$ orbital and 5% of the spin density transferred to the planar hydride ligands.

Preparation and preliminary EPR measurements of a Li_4RhH_5 powder sample are described.

BAND THEORY AND ELECTRONIC STRUCTURE. 17

A unified computer program package was developed to calculate the electronic properties of atoms, molecules, and small clusters of atoms using the Generalized Valence Bond/Unrestricted Hartree-Fock model. Initial tests of these computer codes were sucessfully completed.

SEPARATION CHEMISTRY

ELECTROSTRIPPING SOLUTIONS FOR IRIDIUM. 19

Small amounts of iridium dissolve from iridium anodes when placed in solutions of disodium cyanamide or sodium dicyanamide.

PROTACTINIUM-231 and THORIUM-230. 19

A shipment of 165 mg of protactinium-231 was made to the Isotope Sales at ORNL in fulfillment of the FY-1976 quota. A shipment of 17.1 grams of thorium-230 was made to the ORNL Isotope Sales in fulfillment of the FY-1976A quota; an additional 29.9 grams of thorium-230 is on hand toward the FY-1977 quota.

Page

THORIUM-229 20

A total of 10.87 mg of thorium-229 has been separated from low-purity, aged uranium-233 during this reporting period. An evaluation of the use of the current, larger extraction equipment was initiated to determine the effect of the increased size on extraction efficiency. A General Plant Project was approved with the objective of keeping the uranium-233 in a liquid state at all times.

URANIUM-234. 20

Analyses were completed on uranium-234, product A15-1. Final separation and analyses were completed on uranium-234, product A13-3, which originated from uranium recovered from the processing of product A13-2. Shipments of 20.100 grams of uranium-234 at 95.97% isotopic purity from A15-1, and 5.056 grams of uranium-234 at 99.08% isotopic purity from A13-3, were made to Isotope Sales at ORNL. Initial separation of uranium from plutonium "cow" B14-02 was completed.

SEPARATION RESEARCH

CHLORINE ISOTOPE SEPARATION. 22

Chlorine isotopes were separated by liquid phase thermal diffusion of chlorobenzene in a 15-column cascade. The performance of columns in the chlorine-37 section of the cascade was evaluated and substantial improvement was obtained by reducing the flow rate of the cooling water. The following enriched materials were produced: 14 g of chlorine-35 at 90% enrichment, 24 g of chlorine-35 at 95% enrichment, and 5.4 g of chlorine-37 at 90% enrichment.

Two columns were removed from the cascade for a detailed study of the effect of water flow rate on column performance. The equilibrium separation factor, the initial transport coefficient, and the remixing coefficient were determined at water flow rates up to 5 liters/min. The columns were found to give substantially better performance at very low flow rates.

MOLECULAR BEAM SCATTERING. 26

The quadrupole detector system was installed and tested with computerized signal averaging. A new beam source and target gas cell were built, and work has begun on a velocity selector mounting system for the primary-beam arm of the molecular beam chamber.

TRANSPORT PROPERTIES 29

Low-temperature thermal diffusion factors for the He-3/He-4 system determined in the two-bulb apparatus several years ago were re-examined. The study consisted of extending existing theory to accommodate the given experimental conditions, recomputing the thermal diffusion factors, and estimating experimental uncertainties. Two theoretical helium interaction potentials were compared to the experimental results. Since experimental uncertainty masked the difference between the two potentials down to 4.2 K, the lowest experimental temperature, it was concluded that experiments must be conducted with the cold bulb at a minimum of 2 K in order to resolve the effective difference in the potentials on α_T.

The composition dependence of the thermal diffusion factors for the Ar-Xe and Kr-Xe systems was measured at 250 K. The temperature dependence is also given for the range 250 to 750 K.

Isotope Separation

ARGON

The 13-column, hot wire, thermal diffusion cascade has continued to produce approximately 7% argon-38. This material is being collected and saved for later enrichment to 95%. The system also produced argon-36 at 99.5% enrichment. *(Gilbert E. Stuber)*

CARBON

During this period, methane with a carbon-13 concentration of 99% and containing 19.5 grams of carbon-13 was produced. Carbon dioxide with a carbon-13 concentration of 97% and containing 22.3 grams of carbon-13 was produced. Elemental carbon with a carbon-13 concentration of 97% and containing 78 grams of carbon-13 was produced.

Production and shipment of two special batches of carbon-12 methane were reported previously. Product specifications required that the carbon-13 content be less than 10 ppm relative to total carbon. Results of preliminary experiments with the first batch are now available. No carbon-13 was detected and this material will, therefore, be suitable for the proposed experiments.

Enrichment of a special batch of carbon-13 to 99.9% has been completed. The carbon-13 is in the form of methane, which will have to be carefully purified and then burned to carbon dioxide, which is the chemical form that the customer requires. *(William J. Roos and Jerome C. Liner)*

HELIUM

During this period approximately 4400 STP liters of 99.9% helium-3 was produced. *(Jerome C. Liner and William J. Roos)*

KRYPTON

The nine-column, five-stage thermal diffusion cascade has been used to partially enrich the heavy isotopes of krypton. This material is then fed to a 19-column, eight-stage thermal diffusion cascade where krypton-86 is enriched to 99% in the bottom stream and depleted to less than 8% in the top stream. This top stream has been collected and will be used in the future for the enrichment of krypton-82, -83, and -84.

The 10-column, nine-stage cascade was used to produce a batch of 90% krypton-82 and a batch of 90% krypton-80. The feed gas used for both of these enrichments was krypton, collected and saved from many previous operations, which did not meet any present product specifications. This is the first time either of these isotopes of krypton has been enriched to 90% at Mound Laboratory. *(Gilbert E. Stuber)*

Radiometric Krypton During this period, three batches of krypton, highly depleted in krypton-85, were shipped from Mound Laboratory. Previously, an additional batch of depleted material had been shipped. Also shipped was a quantity of krypton with a somewhat lower krypton-85 depletion factor. ERDA and the customer have agreed that the requirements of the program have been completed. The thermal diffusion system which had been used in this program is now available for use in the inventory program. *(William J. Roos)*

NEON

A six-column, double cascade thermal diffusion system produced approximately 0.5 STP liter of 90% neon-21 during this period.

Upgrading of neon-20 and neon-22 to product grade has continued in a four-column thermal diffusion system. The materials being upgraded are slightly below product specifications. *(Gilbert E. Stuber)*

OXYGEN

The pilot-scale electrolysis system for producing oxygen-16 gas has been completed. The system, which utilizes a General Electric Solid Polymer Electrolyte Water Electrolysis Unit, has been operated and appears to give satisfactory results. This system will now be turned over to oxygen-18 gas production, and the work on a similar large-scale electrolysis system for oxygen-16 will proceed. *(Jerome C. Liner)*

SULFUR

A thorough helium leak check of the sulfur isotopes chemical exchange system and a checkout of system operation with air, water, and nitrogen in place of system chemicals have been completed. Start-up has been delayed due to lack of manpower. *(Regis F. Cmar)*

XENON

During this period a 19-column thermal diffusion system produced approximately 0.65 STP liter of 40% xenon-124; a 24-column system produced approximately 2.5 STP liters of 5% xenon-124 and 1.0 STP liter of 2% xenon-126; and an 8-column system produced approximately 11 STP liters of 80% xenon-136 and a batch of 50% xenon-134. *(William J. Roos)*

Low Temperature Research

VAPOR PRESSURE STUDIES

The measurements of the vapor pressure differences between mixtures of ortho-para deuterium and equilibrium deuterium (2.15% para) have been extended to mixtures with higher concentrations of para molecules. Two 1-liter samples of approximately 80% para-deuterium were obtained from Professor David White of the University of Pennsylvania. Very large and irreproducible time dependent differences were measured against the eD_2 standard. The rate of conversion of the para to the ortho species increases as the square of the concentration of the former. The samples (~80% para) converted markedly (to ~60% para) in two days in the cryostat. This rate of conversion raises questions about the validity of the data. The data will therefore be presented qualitatively rather than quantitatively.

The data can be related to the difference in the free energies of the mixtures through quantity J derived in a previous report.[1] The relationship among the measured quantities ΔP, Pe, T, and J is given by:

$$J = -\ln\left(1 - \frac{\Delta P}{Pe}\right) + \frac{B_{1\cdot1}\Delta P}{RT}, \qquad (1)$$

where B_{11} is the virial coefficient for D_2. From a quantum mechanical model of solid D_2,[2] one would expect $\overline{X-X_e}$ to be a nearly linear function in 1/T for a given $X-X_e$. Since the following data do not follow this model, it was decided to quench the samples from the liquid state to below 10 K and then warm them up.

The first sample had a beginning value of $X-X_e = 0.71$. The first data shown in Figure 1 were taken from 12.5 K to 18.75 K on June 24. The sample was then cooled and kept at 12 K overnight. The sample exhibited completely different behavior above 1/T = 0.65, as shown by the data from June 25. After the re-measurement, X was determined again and $(X-X_e)$ had decreased to 50%.

The 50% $(X-X_e)$ sample was withdrawn, stored, and measured again on July 7, 8 and 9. Figure 2 reproduces the June 25 data alongside the results from the fresh 50% sample on July 7. Below 1/T = 0.066 (T > 15 K), the results on the 50% sample on the two days are the same. In the high 1/T region (T < 15 K), there is a marked difference in the two runs. There is clearly an aging process in the solid which reduces the low temperature-vapor pressure ratio. Note that there is a threshhold for diffusion in solid D_2 at about 15 K.

In the July 7, 8, and 9 run there is a decrease in $(X-X_e)$ with time as seen in Figure 3. The 50% data are the same as in Figure 2. The low temperature aging effect can again be seen but it is not as pronounced as in Figure 2. There is also an evident decrease in the vapor pressure ratio with decreasing $(X-X_e)$. At the time these measurements were made there was a question as to the quality of the sample. There was also a problem in that the first sample had been sublimed into the vapor pressure bulbs rather than condensed because of the low sample pressure. The second sample was then obtained from Prof. White; it was 82% para-deuterium at 1 atm.

The new sample was condensed to a liquid and then cooled to 12 K. The first run-up in temperature to the triple point was taken very fast, six points in one hour, and the results are shown in Figure 4 as data (1) for July 20. The sample remained at a temperature just above the critical point for one-half hour and then was cooled to 11 K. Data was again taken up to the triple point, this time seventeen points in five hours. These points are shown in Figure 4 as data (2) for July 20: they exhibit a minimum like the 37% data in Figure 3. The points measured the next day are relatively linear and the concentration difference was found to be 63%.

A second run using the 82% para sample is represented by the graph in Figure 5. The samples were condensed to liquid and cooled slowly to 11 K; data were then taken up to the triple point. The samples were cooled again to 11 K and maintained overnight. After the July 29 data were taken, the concentration of para species was determined to be 65%.

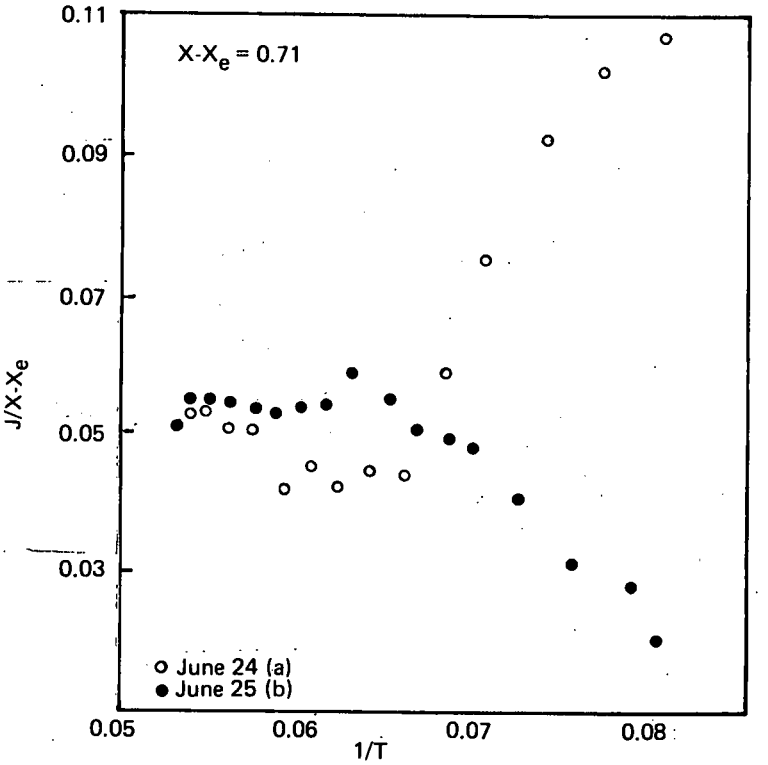

FIGURE 1 - Temperature dependence of ortho-para D_2 mixture vapor pressure ratio after (a) sample quench and (b) anneal overnight.

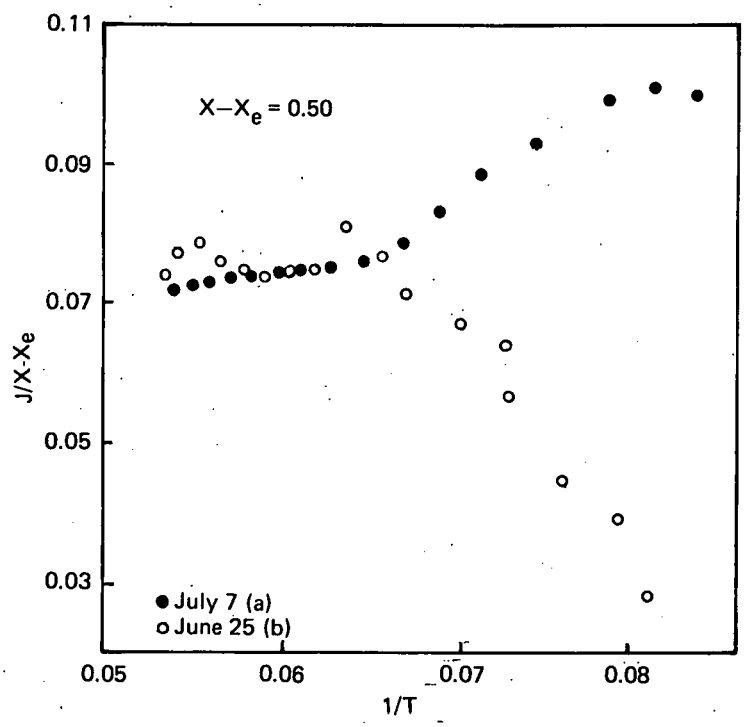

FIGURE 2 - Temperature dependence of ortho-para D_2 mixture vapor pressure ratio after (a) sample slow cool and (b) anneal overnight.

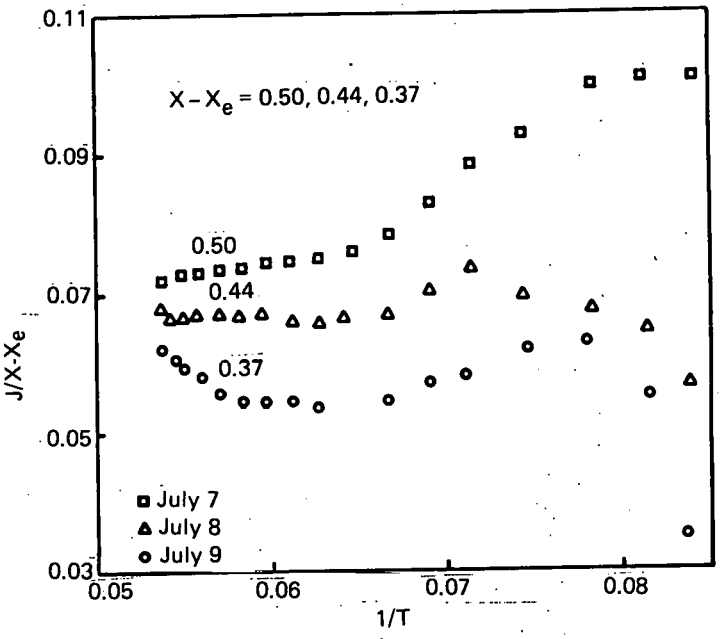

FIGURE 3 - Temperature dependence of ortho-para D_2 mixture vapor pressure ratio after slow cool on three successive days.

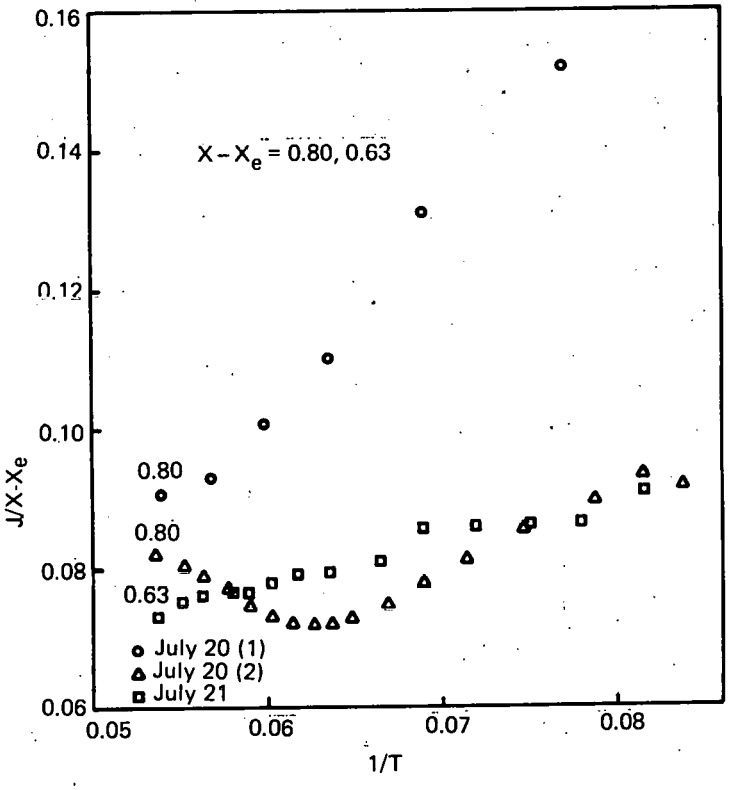

FIGURE 4 - Temperature dependence of ortho-para D_2 mixture vapor pressure ratio, data taken in three different ways (see text).

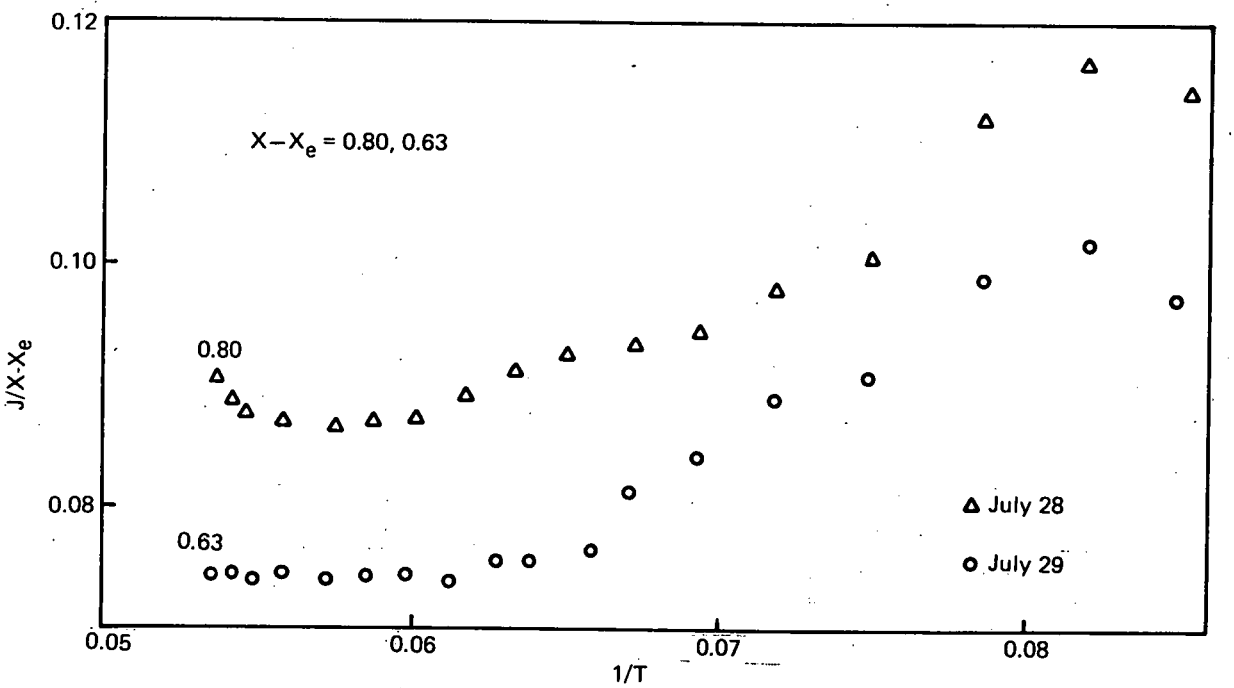

FIGURE 5 - Temperature dependence of ortho-para D_2 mixture vapor pressure ratio after condensing sample as liquid on two successive days.

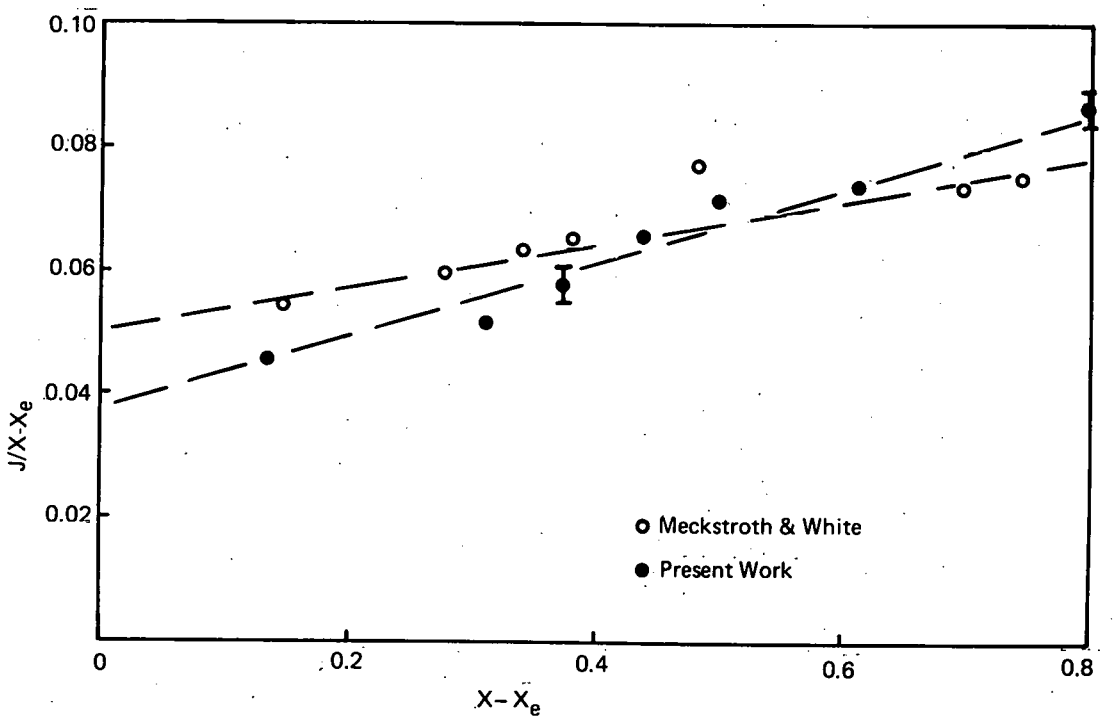

FIGURE 6 - Deuterium vapor pressure ratios compared with published measurements.

These data present several problems. It is quite clear that the conversion of para to ortho species has to be slowed. It is also clear that quenching the samples to the solid produces large unexplainable effects at the low temperature end of the measurement, as seen in Figures 1 and 2. Even when the sample is condensed to a liquid, the results depend on the speed with which the run is taken, as seen in Figure 4. The faster run of July 20 is the only one that produced data comparable with that of Meckstroth and White.[2]

Since the data near the triple point seemed to be the most reproducible, five new data points were added to the graph (see Figure 4 in the last progress report[1]) which compares this work to that of Meckstroth and White. The new data points, i.e., where $X-X_e = 0.37, 0.44, 0.50, 0.63,$ and 0.80, are shown in Figure 6. The slope of the line determined by the new points is greater than that of Meckstroth and White, although at this stage it is not clear whether the difference is slopes is real. As seen from earlier work (Equation 7 in the last progress report[1]), the slope is related to the electric quadrupole constant for solid D_2. *(George T. McConville)*

Metal Hydride Research

PULSE NMR STUDIES

Studies of $TiFeH_x$ A nuclear magnetic resonance (NMR) investigation of the physical properties of β-phase and γ-phase $TiFeH_x$ has continued. The $TiFeH_x$ system is a primary candidate for hydrogen storage applications. Previous pulse NMR measurements have provided some information on the nuclear relaxation times for protons in the $TiFeH_x$ phases.[3] However, analysis and interpretation of these results were complicated by difficulties with both instrumentation and sample properties. Iron and oxygen impurity levels of 0.3% greatly influence the hydride phase composition and magnetic susceptibilities. Consequently, a sample of $Ti_{1.04}Fe_{0.96}H_{2.0}$ was obtained from Dr. G. C. Carter of National Bureau of Standards (NBS). This sample is near the maximum composition for the γ-phase and was prepared from high purity materials with minimum oxygen contaminant. The proton relaxation times T_2^*, T_2', and T_1 were measured between 150 K and 320 K at 34.5 MHz using the previously described techniques.[3] These results can be compared with similar measurements on a sample of γ-phase $TiFeH_{1.7}$ prepared at Mound Laboratory.

The proton line width relaxation time (T_2^*) was 2.9 μs for $Ti_{1.04}Fe_{0.96}H_{2.0}$ (NBS) and 2.6 μs for $TiFeH_{1.7}$ (Mound). This suggests a somewhat lower magnetic impurity content in the NBS sample; however, there is still a high enough magnetic susceptibility to interfere with the NMR measurements. The small T_2^* values are caused not only by intrinsic bulk susceptibility from the paramagnetic lattice but also by at least two extrinsic factors (i.e., excess iron and a ferromagnetic surface film formed by exposure of $TiFeH_x$ to air as a stabilization technique). The slightly larger T_2^* for the NBS sample, which contained an excess of titanium, seems to indicate that the surface film is more important than the excess iron in producing the nonhomogeneous magnetic field. The dependence of bulk magnetic susceptibility on $TiFeH_x$ phase composition must still be determined.

The temperature dependence of the proton spin-spin relaxation time, T_2', for $Ti_{1.04}Fe_{0.96}H_{2.0}$ is shown in Figure 7. Here, T_2' is nearly independent of temperature with an average value of 36 ± 3 μs, which is in excellent agreement with the value for $TiFeH_{1.7}$ obtained earlier.[3] The slight decrease with temperature observed in Figure 7 is within experimental uncertainty, but it may be the result of an esoteric relaxation mechanism for the highly paramagnetic $TiFeH_x$. This possibility is currently being evaluated. However, the equivalent T_2' values for the Mound and NBS samples indicate that the arrangement of hydrogen atoms is identical (i.e., both samples are γ-phase $TiFeH_{\sim 2}$). Furthermore, the absence of a T_2' increase at higher temperatures verifies the previous conclusion that hydrogen mobility in γ-phase $TiFeH_x$ is too slow to significantly reduce the dipolar interactions between rigid spins.[3] This finding leads to an upper limit of $<10^{-11}$ cm^2/s for the hydrogen diffusion constant at room temperature.[4]

The spin-lattice relaxation (T_1) has also been measured for the NBS sample of $Ti_{1.04}Fe_{0.96}H_{2.0}$. A plot of $1/T_1$ versus temperature is given in Figure 8 where T_1 obeys the Korringa relation:

$$T_1T = C_K,$$

with $C_K = 5.4$ sK. Similar behavior was

found for T_1 in the $TiFeH_{1.7}$ sample prepared at Mound, where $C_K = 5.6 \pm 0.4$. Since C_K is related to the density of electronic states at the Fermi energy, these results imply that the electronic structures of these two samples are nearly the same and that both samples represent γ-phase $TiFeH_{\sim 2}$. Unfortunately, the C_K data alone is unable to provide an understanding of the electronic structure of γ-phase $TiFeH_{\sim 2}$. However, a significant difference between the electronic structures of the γ and β phases is indicated since C_K for β-phase $TiFeH_{1.0}$ has been reported as 3.0 ± 0.3 sK.[3]

In conclusion, the recent measurements on the NBS sample tend to verify the earlier observations on the spin relaxation properties for γ-phase $TiFeH_{1.7}$ samples prepared at Mound. With an increased confidence in the experimental approach, further studies of the $TiFeH_X$ system are in progress. Immediate attention is directed toward determining whether the hydrogen mobility in the β-phase causes motional narrowing[4] (i.e., increase in T_2') above ~350 K as reported by Carter and Chabre (private communication with D. C. Carter).

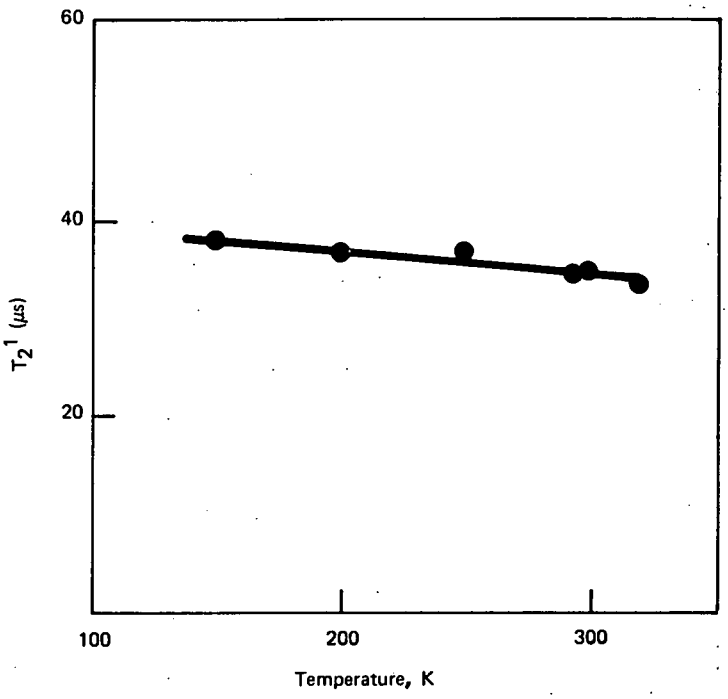

FIGURE 7 - Proton spin-spin relaxation rates in γ-phase $Ti_{1.04}Fe_{0.96}H_{2.0}$.

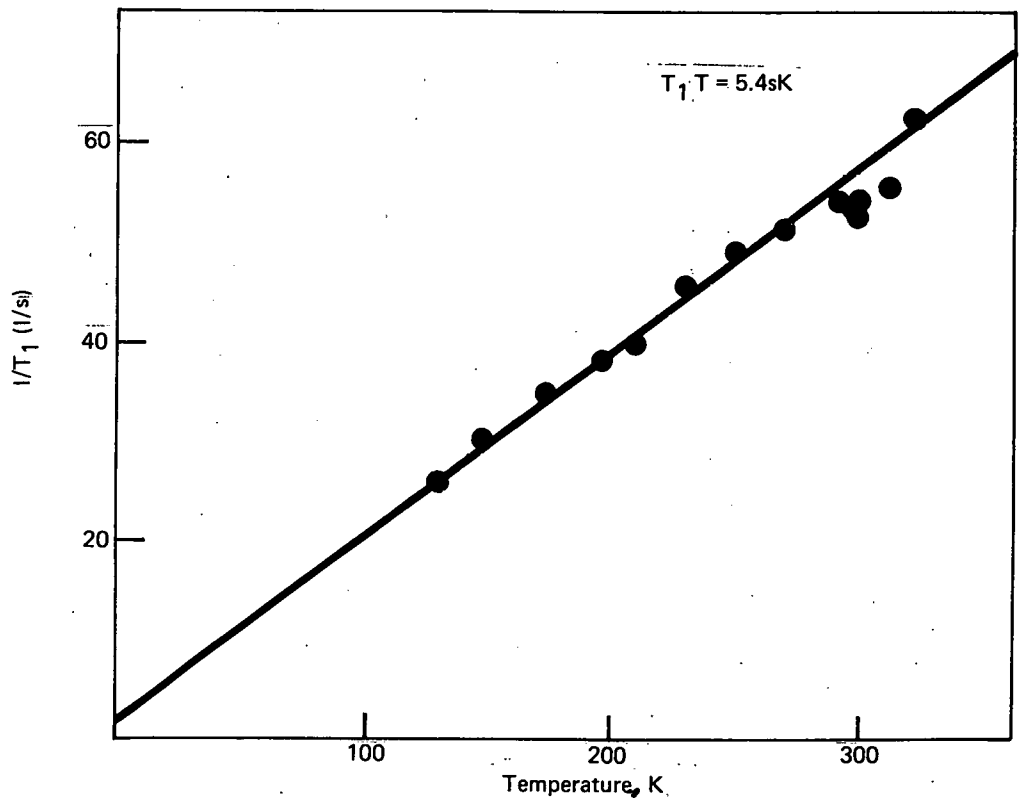

FIGURE 8 - Proton spin-lattice relaxation rates in γ-phase $Ti_{1.04}Fe_{0.96}H_{2.0}$.

Low Temperature Hydrogen Ordering in VH_x

The interrelationships between phase formation, stability, electronic structure, hydrogen lattice site occupancies, and hydrogen mobility are being investigated in order to better characterize metal hydrides for energy storage applications. Isotope substitution does not seem to significantly influence either phase formation or structure in several metal hydride systems, including uranium, titanium, lithium, and tantalum hydrides. However, recent studies[5-11] indicate a surprisingly great difference in the phase diagrams of the V-H and V-D systems. Briefly, these differences include:

1) At room temperature the body-centered-tetragonal (bct) β-phase exists for VH_x compositions between x = 0.4 and 0.9 while β-phase VD_x exists only between $VD_{0.45}$ and $VD_{0.55}$. A body-centered-cubic (bcc) phase forms for compositions above $VD_{0.55}$ and exists to temperatures as low as 80 K.

2) The β-α transition for VD_x occurs at a 50-90 K lower temperature than for VH_x.

3) A phase change that occurs near ~200 K for β-phase VH_x is not observed for β-phase VD_x.

Structural characterizations of the distorted bcc VH_x and VD_x phases are complicated by the existence of twelve tetrahedral and six octrahedral sites per unit cell. Stalinski has discussed three tentative models[12] of the ordered $VH(D)_{1.0}$ structures:

I. bct H-sublattice in octahedral sites,
II. bct H-sublattice in tetrahedral sites, and
III. orthorhombic H-sublattice in tetrahedral sites.

In addition, selective occupancy of these sites results in ordered superstructures for V_4H_2, V_6H_4 and V_8H_6. Neutron diffraction[7,9] and NMR studies of the deuteron quadrupole splittings[11] have established the occupied deuterium lattice sites in the VD_x phases. These results are summarized in Table 1. Unfortunately, neither these techniques nor X-ray diffraction[5,6] and electron diffraction[13] can locate the hydrogen atoms in the VH_x phases.

In principle, the dipole-dipole interactions in the proton NMR line shape will provide information on the hydrogen lattice sites through the second moment, M_{2D}, where:

$$M_{2D} = M_{2H} + M_{2V}$$
$$= \frac{3}{5}\hbar^2 \gamma_I^2 I (I+1) f_I \sum_i r_i^{-6}$$
$$= \frac{4}{15}\hbar^2 \gamma_S^2 S (S+1) f_S \sum_j r_j^{-6} \quad (1)$$

Here, $\hbar$ is Planck's constant divided by 2π; γ_I and γ_S are the gyromagnetic ratios for protium (I = 1/2) and vanadium (S = 7/2); f_I and f_S are the fractional site occupancies of H and V spins; and the lattice sums, $\sum_i r_i^{-6}$ and $\sum_j r_j^{-6}$, for the occupied H and V lattice sites respectively, contain the structural information. Since $M_{2V} >> M_{2H}$ for any possible structure of bcc or bct VH_x phase, the total M_{2D}, as obtained from the continuous-wave spectrum, free induction decay, or solid echo, cannot be adequately analyzed to accurately determine the occupied hydrogen lattice sites. However, it is possible to determine only M_{2H} using the $\pi/2$-τ-π spin echo pulse sequence[14,15] when $E(\tau)$, the ratio of the echo maximum for pulse spacing (τ) to the extrapolated maximum at $\tau = 0$, obeys the following:

$$E(\tau) = 1 - M_{2H}\frac{(2\tau)^2}{2!} + M_{4\epsilon}\frac{(2\tau)^4}{4!} - M_{6\epsilon}\frac{(2\tau)^6}{6!} + \ldots \quad (2)$$

Table 1

CRYSTALLOGRAPHIC DATA OF THE V-D ALLOYS*

Phase	Metal Lattice	Deuterium Site Occupancies	Unit Cell Symmetry	Space Group	Unit Cell Formula
α	bcc	Disordered in tetrahedral sites	Cubic	Im3m	--
β	bct	Ordered in octahedral sites	Monoclinic	Cm	V_4D_2
γ	bcc	Ordered in tetrahedral sites	Orthorhombic	Pcc2	V_8D_6
δ	bcc	Ordered in tetrahedral sites	Orthorhombic	Pnnn	V_4D_4

*from references 7, 9, and 11.

and $M_{4\epsilon}$ and $M_{6\epsilon}$ are the fourth- and sixth-moment error terms. If the echo decay train shows Gaussian behavior, Eq. 2 becomes

$$E(\tau) = \exp\left[-\frac{1}{2} M_{2H} (2\tau)^2\right] \qquad (3)$$

and the H-H contribution to the proton second moment can be directly determined.

The proton spin echoes generated with the $\pi/2$-τ-π pulse sequence have been measured at temperatures below 200 K for VH_x compositions between x = 0.39 and x = 1.03. The experiments were performed at 34.5 MHz on a Bruker BKR-323s pulse spectrometer using a Biomation 8100 transient recorder and Nicolet 1074 computer for signal enhancement and background subtraction. Representative proton spin echo trains are presented in Figure 9 for $VH_{0.50}$ and $VH_{0.88}$. The envelopes of echo maxima exhibit Gaussian behavior over at least 85-90% of their decay; hence, the M_{2H} values are readily obtained from Eq. 3.

The M_{2H} values obtained for VH_x from spin echo measurements at 100 K (i.e., the lowest temperature which is reproducible to ±5 K in the apparatus) are summarized in Figure 10. Proton spin-lattice relaxation times and line widths indicate that hydrogen diffusion in VH_x should be extremely slow at this temperature; hence, the experimental M_{2H} should represent only the static interactions between hydrogen spins. The dipolar M_{2H} values calculated with Eq. 1 for the three structural models discussed by Stalinski as well as for the ordered superstructures V_4D_2,[7] V_8D_6,[7] and V_6H_4,[8] are also presented in Figure 10. These calculations were performed assuming random occupancy of the hydrogen lattice sites for compositions below $VH_{1.0}$ (except for the V_4H_2, V_6H_4, and V_8H_6 superstructures where f_I = 1.0) and using the measured lattice constants[11] for $VH_{0.5}$ at 100 K. For VH_x compositions other than $VH_{0.50}$ and $VH_{0.70}$, the lattice constants at ~100 K are unknown.[16]

It is obvious from Figure 10 that Models I, II, and III as well as the ordered superstructures all predict M_{2H} significantly larger than obtained from the $\pi/2$-τ-π pulse sequence. Since both motional narrowing and spin exchange are unlikely major contributors to the M_{2H} values at ~100 K, this large difference between the dipolar and experimental moments implies that none of these models for the hydrogen lattice corresponds to VH_x structure at this temperature. In fact, other studies[8,16,17] indicate β-VH_x

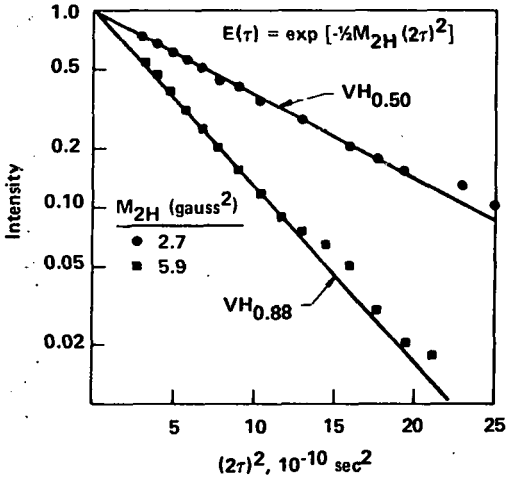

FIGURE 9 - The $\pi/2$-τ-π maximum echo amplitude $E(\tau)$ for protons in $VH_{0.50}$ and $VH_{0.88}$ at 100 K.

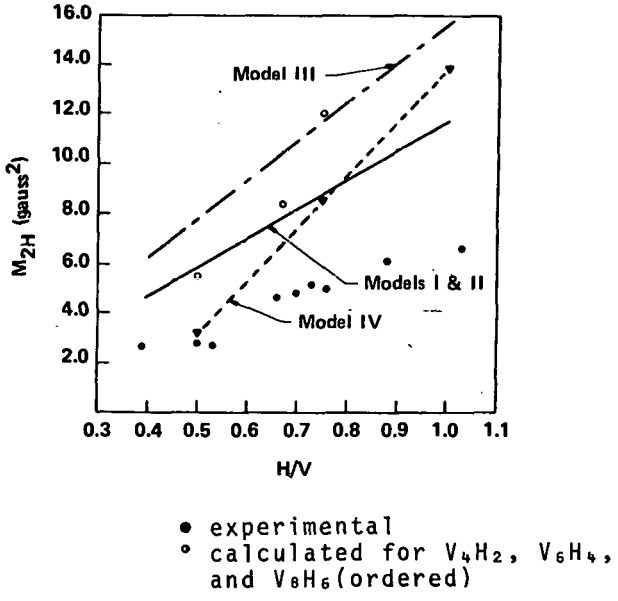

FIGURE 10 - Dipolar moments for VH_x at ~100 K compared to values calculated for Models I and II (random), Model III (random), and Model IV (ordered).

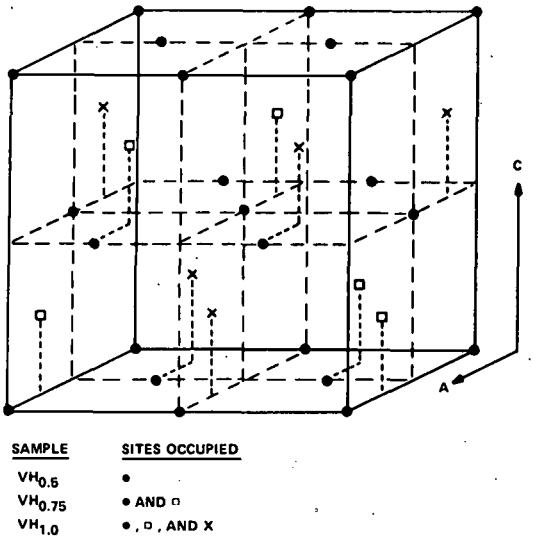

FIGURE 11 - Proposed arrangement of hydrogen atoms (Model IV) in VH_x phases at temperatures below ~200 K.

(which is isomorphic[11] with β-$VD_{0.5}$) undergoes a phase transformation below ~200 K and the hydrogen atoms occupy different interstitial sites.[10] This phase transformation has not been observed for β-VD_x. Consequently, dipolar M_{2H} values have been calculated for several other possible hydrogen arrangements in bct VH_x. The best agreement between calculated and experimental M_{2H} for $VH_{0.5}$ (where measured lattice parameters are available) is obtained with Model IV illustrated in Figure 11. This hydrogen arrangement provides the maximum separation between hydrogen atoms for $VH_{0.5}$. Model IV predicts that M_{2H} will increase rapidly for compositions above $VH_{0.5}$; however, elongation of the tetragonal axis ratio will greatly reduce this increase in M_{2H}. Since the lattice parameters at ~100 K are unknown for compositions near $VH_{1.0}$, the calculated M_{2H} values for these compositions are not reliable, and accurate comparisons between the various models are not currently possible. However, the models can be evaluated for $VH_{0.50}$ and $VH_{0.70}$ since the lattice parameters are known[11,16] near ~100 K. The calculated dipolar moments for several of the models for hydrogen site occupancies in $VH_{0.50}$ and $VH_{0.70}$ are given with the experimental M_{2H} values in Table 2. Model IV clearly gives the best agreement with the spin

Table 2

COMPARISON OF CALCULATED AND EXPERIMENTAL M_{2H} VALUES

Source	M_{2H} (gauss^2) $VH_{0.50}$	$VH_{0.70}$
Model I or II	5.9	7.7
V_4D_2 Model	5.5_5	---
V_8D_6 Model	---	10.3
Model IV	3.2	7.0
Spin Echo (~100 K)	2.8±0.3	4.9±0.5

echo measurements. However, some discrepancy still remains, particularly for $VH_{0.70}$. Several possible explanations include:

1. Residual hydrogen motion - perhaps localized hopping between adjacent sites (this seems unlikely for $VH_{0.50}$ since the experimental M_{2H} was essentially constant below ~200 K).
2. Partially disordered lattice through occupancy of two types of interstitial sites or incomplete phase transformation.[16]
3. Uncertainties in the lattice parameters at ~100 K used to calculate the dipolar M_{2H} values.
4. Errors in the experimental procedures (i.e., pulse widths, timing, background correction, etc.), although these are believed to be <10-20%.

Nevertheless, the present proton spin echo studies strongly indicate that the arrangement of hydrogen atoms in VH_x near ~100 K is not described by the proposed models for the VD_x superstructures.

Model IV as described in Figure 11 is proposed as an alternative arrangement of hydrogen atoms in VH_x at low temperatures. This model cannot distinguish between tetrahedral or octahedral lattice site occupancies from M_{2H} data alone. However, vanadium quadrupole splittings obtained by Arons et al.[10] indicate the normal octahedral sites of the β-phase are not occupied below ~200 K in VH_x.

Future work on the low temperature structure of VH_x will include X-ray diffraction measurements of the concentration dependence of the lattice parameters at ~100 K. In addition, the NMR techniques will be refined, if possible, to improve

the accuracy of the experimental M_{2H} data. *(Robert C. Bowman, Jr. and Albert Attalla)*

ELECTRON PARAMAGNETIC RESONANCE STUDIES OF TRANSITION METAL IONS IN METAL HYDRIDES

Electron paramagnetic resonance (EPR) studies of transition metal and rare earth ions in diamagnetic metal hydrides have been undertaken to obtain a better understanding of metal-hydrogen chemical bonding. Trends in the covalent contribution to the metal-hydrogen bonds are investigated by analyzing magnetic g-factors and hyperfine constants of paramagnetic impurity ions in binary and ternary hydrides where the bonding characteristics vary from ionic to metallic.

Rhodium Ions in LiH and LiD Single Crystals The previous progress report described EPR spectra for two paramagnetic rhodium (Rh) centers in single crystals of LiH and LiD after ultraviolet irradiation.[18] Species A with orthorhombic symmetry was observed between 77 K and ~120 K, where the short spin-lattice relaxation time produced excessive line-broadening and a disappearance of the EPR spectra above 120 K. A Rh-center having axial symmetry (Species B) was detected between 77 K and 325 K. A preliminary analysis[18] of the g-factors for Species B indicated the rhodium oxidation state was either Rh^{+2} ($4d^7$) or Rh^0 ($4d^9$) with the paramagnetic electron primarily occupying the $d_{x^2-y^2}$ molecular orbital. Evidence for covalent bonding between Rh and the hydride ligands was provided by the presence of super-hyperfine (shf) lines in the EPR spectra for Rh-doped LiH crystals.

During the past several months, more detailed analysis of Species B has indicated that the spin Hamiltonian (H) for this S = 1/2 axial complex is:

$$H = \beta\bar{S}\cdot\bar{g}\cdot\bar{H} + \bar{S}\cdot\bar{A}_{Rh}\cdot\bar{I}_{Rh} + \sum_{n=1}^{6} (\bar{S}\cdot\bar{A}_n - g_N\beta_N\bar{H})\cdot\bar{I}_n \qquad (1)$$

where $\bar{A}_{Rh}$ is the Rh hyperfine tensor; $\bar{A}_n$ and $\bar{I}_n$ are shf tensors and nuclear spin operators, respectively, of the nearest-neighbor nuclei; and the other terms have their usual meanings.[19]

The LiD complex shows no shf effects and the last term in Eq. 1 can be ignored. The values obtained for the phenomenological parameters are: $g_{\parallel} = 2.112$; $g_{\perp} = 2.038$; $A_{Rh} = 26.2 \times 10^{-4}$ cm^{-1}; and $B_{Rh} = 14.5 \times 10^{-4}$ cm^{-1}; where A_{Rh} and B_{Rh} are, respectively, the magnitudes of the parallel and perpendicular components of $\bar{A}_{Rh}$.

The observed g-values and Rh hyperfine constants are consistent with either a Rh^{+2} ($4d^7$) or Rh^0 ($4d^9$) paramagnetic ion.[19] Since $g_{\parallel} > g_{\perp} > 2.0$, the paramagnetic electron belongs to the $4d_{x^2-y^2}$ orbital. The observed hyperfine constants give $\chi = -5.22$ a.u. (atomic units) for the core polarization parameter, favoring the Rh^{+2} configuration.[20]

For the LiH complex, the shf terms of Eq. 1 are important; unfortunately the proton Zeeman term is comparable with the proton hyperfine interaction, giving rise to satellite lines[19] that cause extensive interference and poor resolution. However, when H is along a principal axis, the satellites disappear and simple expressions for resonance apply. When H is along the z-axis ($H_{\parallel}$), then

$$H_{res} = [h\nu \pm 0.5A_{Rh} + A_{1z}(m_x + m_y) + A_{3z}m_z]/g_{\parallel}\beta, \qquad (2)$$

and when H is along the x- or y-axis ($H_{\perp}$), then

$$H_{res} = [h\nu \pm 0.5B_{Rh} + A_{1x}m_x + A_{2x}m_y + A_{3x}m_z]/g_{\perp}\beta. \qquad (3)$$

In Eq. 2 and 3, A_{nq} is the magnitude of the component of $\bar{A}_n$ along the q-principal axis, while $m_x = m_1 + m_4$, $m_y = m_2 + m_5$, and $m_z = m_3 + m_6$ are nuclear spin magnetic quantum numbers for nearest-neighbor protons along the positive and negative x-, y-, and z-axes, respectively. The observed shf splittings are consistent with $A_{1x} = 14.7$; $A_{3z} \leq 5.5$; and A_{3x}, A_{2x}, $A_{1z} \leq 4.5$ in units of 10^{-4} cm^{-1}. This is the only solution compatible with the theory (vide infra). Since $A_{1x} \cong B_{Rh}$, the shf pattern at $H_{\perp}$ appears as a 1:3:3:1 (intensity ratio) quartet.

The observed shf structure of the LiH complex can be explained by assigning the paramagnetic electron to the molecular orbital[19] $\psi = \sqrt{N^{-1}}[4d_{x^2-y^2} - \lambda(\sigma_1 + \sigma_4 - \sigma_2 - \sigma_5)/2]$, where σ is the hydrogen 1s-orbital and N is a normalization constant. Through this participation, each ligand in the xy-plane contributes an isotropic shf term, $A_s = f_{\sigma}a_s$, where $f_{\sigma} = \lambda^2/4N$ is the paramagnetic spin density transferred to each xy-ligand and $a_s = 474 \times 10^{-4}$ cm^{-1} is the hydrogen 1s hyperfine coupling constant.

There are also anisotropic shf terms due to the dipolar interaction of the nuclear moment of each ligand with the distribution of magnetization carried by the $4d_{x^2-y^2}$ orbital. Marshall[21] derived a general solution of this problem for various transition ion complexes. His results for a d^9 ion with a hole in the $d_{x^2-y^2}$ orbital (also applicable to a strong field d^7 ion with an electron in $d_{x^2-y^2}$) provide the following expressions: $A_{1x} = A_s + 2A_d[1 + 6\langle\rho^2\rangle/7 + 95\langle\rho^4\rangle/28]$; $A_{2x} = A_s - A_dX\ [1 + 3\langle\rho^2\rangle/7 + 125\langle\rho^4\rangle/28]$; and $A_{3z} = 2A_d[1 - 12\langle\rho^2\rangle/7 + 5\langle\rho^4\rangle/7]$ while $A_{1z} \cong A_{2x}$ and $A_{3x} = -0.5A_{3z}$. In these expressions $A_d = g_e\beta g_N\beta_N R^{-3}$ and $\rho = r/R$, where r is the electron radius about the central ion and R is the central ion-ligand internuclear separation.

In the usual approximation for the dipolar interaction[19] the terms in brackets are replaced by unity; however, in the present case these terms produce a considerable effect, not only on the absolute magnitude of the shf parameters but also on their relative magnitudes.

Taking R = 3.85 a.u. (the LiH internuclear separation), and using free ion values[19] for Rh^{2+} of $\langle r^2\rangle$ = 2.374 a.u. and $\langle r^4\rangle$ = 10.60 a.u., the dipolar terms can be calculated, giving: $A_{1x} = A_s + 8.12$; $A_{2x} = A_s - 4.01$; $A_{3z} = 4.7$ in units of 10^{-4} cm^{-1}. This agrees with the observed values when $A_s = 6.6 \pm 0.7$, giving $4f_\sigma = 0.056 \pm 0.006$ for the total magnetic spin density on the xy-ligands.

Future work on this system will include: 1) a more detailed characterization of the orthorhombic species A, and 2) comparison of rhodium g-factors and hyperfine constants for LiH and LiD with published data for Rh^{+2} ions in other crystal systems. This study should provide an improved assessment of both crystal field and covalent bonding contributions.

Studies of Li_4RhH_5 and Li_4RhH_4 The primary objective for EPR studies of metal hydrides is to determine differences in the metal-hydrogen bonding parameters as the hydride properties change from ionic to metallic. Since EPR spectra are observed for paramagnetic Rh ions in LiH crystals, similar Rh centers may be formed in the ternary hydrides Li_4RhH_4 and Li_4RhH_5. These hydrides, which are structurally related[22] to LiH, have physical properties indicating metallic character. Hence, Li_4RhH_4 and Li_4RhH_5 provide a potential opportunity of extending the observations for Rh ions in ionic LiH, to similar systems with properties resembling transition metal hydrides.

It was decided first to prepare and examine a sample of Li_4RhH_5, which has properties of a semiconductor and is more closely related[22] to the LiH-Rh system. The possibility of producing paramagnetic Rh ions may be greater in Li_4RhH_5 since Rh has a formal oxidation state of +1 and the rhodium-rhodium bonding suggested[22] for Li_4RhH_4 is absent. The synthesis procedure described by Lundberg[23] was used where the stoichiometric mixture 4LiH + Rh (metal) was heated to ~873 K (~600°C) with H_2 gas at 241 kPa (35 psia) pressure. A reaction occurred with a subsequent pressure drop to 165 kPa (24 psia). Unfortunately, volumetric-mass spectrometric analysis on the "LiH" powder indicated the actual composition was $LiH_{0.8}D_{0.2}$ which resulted in an error in the mixture composition. The product Li_4RhH_5 is slightly rich in Rh.

Some preliminary EPR measurements were performed on a powder sample of this Li_4RhH_5 product. A weak, narrow (ΔH~1-2 gauss) peak, probably due to lithium metal impurities, and a possibly weak and very broad ($\Delta H \gtrsim 1000$ gauss) absorption were the only EPR spectra found in this sample. Measurements were performed at room temperature and with the sample cooled in liquid argon. In addition, room temperature irradiation for several minutes with an unfiltered mercury lamp had no noticeable effect on the EPR spectra. The $Rh^{+1}(4d^8)$ ion in pseudocubic symmetry, which Lundberg et al.[22] have suggested as the possible Rh species in Li_4RhH_5, may be responsible for the very broad EPR spectra. The Li_4RhH_5 sample did not show EPR spectra corresponding to species A and B in Rh-doped LiH. A more severe form of irradiation (i.e., X-rays) may give rise to the Rh^{+2} species in Li_4RhH_5. Another sample of Li_4RhH_5 will be prepared after a new batch of LiH is synthesized. Careful sample handling and various irradiation techniques will be used in the attempt to produce paramagnetic Rh centers. *(George C. Abell, Robert C. Bowman, Jr., and Calvin M. Love)*

BAND THEORY AND ELECTRONIC STRUCTURE

At Mound Laboratory a unified package of computer programs for the ab initio calculation of electronic properties of atoms, molecules, and small clusters of atoms has been successfully developed. This package makes it possible to calculate electronic properties within the open-shell (restricted) Hartree-Fock, the Generalized Valence Bond, and the unrestricted Hartree-Fock (UHF) schemes. The package consists of four major parts:

1) the BIGGMOLI molecular integrals programs BMO1O and BMO20 written by Dr. R. C. Raffenetti (NASA, Langley);

2) the integral processing programs BIGPLY, PLYIJLK, and PLYPAIR written by Dr. F. W. Bobrowicz, now of Mound Laboratory;

3) the generalized self-consistent field (SCF) programs, GENSCF, by Bobrowicz for performing open-shell Hartree-Fock and/or Generalized Valence Bond calculations of electronic wave functions; and,

4) the unrestricted Hartree-Fock SCF programs, UHFSCF, by Bobrowicz.

The output files from the integrals programs are acceptable both to the GENSCF and to the UHFSCF programs.

A period of testing of the present codes has been completed. During this period it has been possible to compare, in a limited manner, the present program package with previous unrestricted Hartree-Fock programs of Prof. A. B. Kunz of the Univ. of Illinois (Urbana), and Dr. R. N. Euwema of Battelle Laboratory (Columbus). In selected test cases, agreement was obtained among all three sets of UHF codes. This, of course, is a check not only upon the SCF portion of the codes, but also upon the integrals calculation and the integrals processing portions. All three sets of codes are completely different and share no common parts. The advantages of the present version, however, are (1) the improved efficiencies, both of the integrals calculation and of the basis function representation, because of the use of the BIGGMOLI code, and (2) the unified treatment of open-shell restricted and unrestricted Hartree-Fock codes.

The output from the open-shell Hartree-Fock and the Generalized Valence Bond programs can be used as input to MCSCF (multi-configuration self-consistent field) or CI (configuration interaction) programs, if desired. But, because of the use of different computers and compilers for the three different programs, it has not yet been possible to compare timing in detail. Also the advantages to be gained by the integral processing schemes of the present programs will not become apparent until test cases involving several metal atoms are studied.

Since the objective of this computer program development is to obtain a computational research tool for the investigation of the effects of hydrogen in metals, the direction set at Mound Laboratory is toward a balance between the computational (and physical) accuracy of a model and the computational expense. It is, therefore, not expected that a major effort will be expended toward the use of such relatively powerful techniques as MCSCF and CI for the Metal-Hydrogen Program. Rather, the major effort is to be directed at the Hartree-Fock level, both restricted and unrestricted. The use of MCSCF and CI is to be considered for small numbers of metal atoms for a basic understanding of metal-metal interactions. However, these techniques are prohibitively difficult and expensive for more than two or three metal atoms.

The major activity of the next several months will be the implementation of an "effective potentials" computer code within the current package of programs. This will allow the calculation of much larger clusters of atoms because it can be used to reduce the number of electrons in a system under consideration to only the valence electrons. The relatively small decrease in computational accuracy is far outweighed by the decrease in computer time and memory requirements.

With this additional code it will be possible to embark upon the actual calculation of selected systems of interest. The initial subject of these programs will be small numbers of scandium and titanium atoms with and without hydrogen atoms. The direct results will be such information as (1) metal-metal and metal-hydrogen bonding mechanisms, (2) hydrogen-hydrogen interactions within a metal lattice, (3) hydrogen diffusion within a metal lattice, and (4) interactions of hydrogen atoms and molecules with a metallic surface. *(Jerry L. Ivey)*

Separation Chemistry

ELECTROSTRIPPING SOLUTIONS FOR IRIDIUM

It is often desirable to strip or polish the surface of iridium metal for various applications, such as transmission electron microscopy, for which Murr has suggested a 2M potassium cyanide solution.[24] A disadvantage of this procedure is that potassium cyanide is a very poisonous chemical. Several recent experiments aimed at dissolving iridium metal anodically have pointed to solutions of sodium dicyanamide, $NaN(CN)_2$, and disodium cyanamide, Na_2NCN, as new electropolishing solutions for iridium. Not only are these materials much less toxic and dangerous than potassium cyanide, but they also can be used for the anodic dissolution of much smaller quantities of iridium. For example, when a strip of metallic iridium about 3 cm long and 0.3 cm wide was immersed into a $NaN(CN)_2$ solution [100 ml of solution containing 10 g of $NaN(CN)_2$] as the anode and electrolyzed at a total current of 1 A for 5 min, the resulting 100-ml solution contained iridium to the extent of 27 μg/ml. Similarly, the same piece of iridium when immersed in 100 ml of a solution containing 11 g of Na_2NCN and electrolyzed at 3 A for 5 min, gave a solution with iridium concentration of 32 μg/ml. In comparison, a $NaN(CN)_2$ solution (5 g per 100 ml) was hardly effective for platinum: a strip of platinum electrolyzed as the anode at 1 A for 5 min dissolved only to the extent of 2 μg/ml. *(Gary L. Silver)*

PROTACTINIUM-231 AND THORIUM-230

Mound Laboratory recovers thorium-230 and protactinium-231 from a uranium mill by-product known as Cotter Concentrate and ships the products to Isotope Sales at ORNL. Previous reports contain detailed descriptions of the origin and character of the Cotter Concentrate, the facilities, and the development of the current recovery and purification process.[25-29] One change during this period was that piping and pipe fittings on one of the Karr extraction columns were changed from plastic to stainless steel.

Briefly, the process consists of leaching approximately 20-liter batches of the solids with hot, concentrated HNO_3 and then diluting and filtering off the insoluble residue. Uranium is removed from the 90-liter batches of filtrate by liquid-liquid extraction with 10% DSBPP/CCl_4 (di-sec-butylphenylphosphonate in carbon tetrachloride) after which it is stripped from the organic with 0.005M HNO_3. Thorium is extracted from the filtrate by multiple contacts with 0.1M TOPO/CCl_4 (tri-*n*-octylphosphine oxide in carbon tetrachloride) with each contact followed by a 0.3M H_2SO_4 strip. After the thorium has been removed from the filtrate, further contacts with TOPO/CCl_4, each followed by an 0.5M oxalic acid strip, result in recovery of the protactinium. Uranium strip solutions are precipitated with ammonia and the precipitate collected for eventual return to the uranium processor. The thorium strip solutions are purified by oxalate precipitation and calcined to the oxide. Protactinium strip solutions are concentrated by evaporation after which they are purified by a series of precipitation steps.

Cotter Concentrate, previously stored in Colorado, was redrummed and 1237 drums were moved to Mound Laboratory for storage pending processing. Since the last semiannual report,[29] 20 additional batches of Cotter Concentrate have been processed from Drums 180, 168 and 169. A shipment of 17.1 g of purified thorium-230 was made to Isotope Sales at ORNL, completing the FY-1976A inventory quota. Thorium purity was equal to that of previous shipments. In addition, 29.9 g of partially purified thorium-230 are on hand from recent production.

A shipment of 165 mg of protactinium-231 was made to the Isotope Sales at ORNL. The recovery and purification of this material was described in earlier reports.[28,29] The shipping value was based on alpha counting of a solution, corrected for losses in the conversion to oxide and for a small contribution of alpha-emitting daughter isotopes. Impurity analyses by emission spectroscopy indicated some iron impurity, and possibly nickel. The oxide had a slight brown color. Total weight of the oxide was 211 mg. Unpurified protactinium-231 recovered from the 20 batches is estimated by gamma spectrum analysis to be 109 mg.

An improved protactinium purification process is being developed and tested, based on additional cycles of TOPO

extraction. Evaporation of oxalate strip solutions produced concentrates of 3-7M HNO_3. Prior experience with the processing of Cotter Concentrate had indicated that extraction of the protactinium into TOPO improved as the acid concentration increased, while the extraction of thorium decreased. The high acidities were undesirable for the previously used phosphate precipitation method, so the TOPO extraction seems to have several advantages.

Five evaporation solutions totaling 8.6 liters and containing 50 mg protactinium are being used to test the TOPO extraction. Processing and process development have not been completed, but the results are encouraging. Under the best conditions, 90% of the protactinium was extracted from a 600-ml aqueous solution into 200 ml of 0.1M TOPO/Amsco* during a 5-minute contact period. Attempts to extract from 3-4M HNO_3 gave extractions of 50% or less under the same conditions. Stripping with 0.5M oxalic acid was used at first, but sometimes resulted in a precipitate which was difficult to separate from the organic phase. Dilute (0.075M) HF was found to strip the protactinium without problems. Following the HF strip, the organic phase was regenerated by stripping with 0.25M sodium carbonate solution (a precipitate often formed) and washing with water twice. The stripped organic was contacted with 7M HNO_3 before reuse. Hydrofluoric strip solutions are currently being concentrated by precipitation with caustic. The sizes of the resulting precipitates were variable and seemed to be related to the magnitude of problems encountered during the extraction steps. Eventually the protactinium will be converted to sulfuric acid medium for additional purification by either DIBC (di-iso-butylcarbinol) extraction or recrystallization of the protactinium from sulfuric acid.
(Paul E. Figgins and Martin R. Hertz)

THORIUM-229

A total of 10.87 mg of thorium-229 has been extracted and purified since the last semiannual report. One shipment, designated LP-3 and made in June 1976, completed the FY-1976 requirement. This shipment contained 3.47 mg of thorium-229. The designation "LP" indicates low purity, or material not previously processed at Mound Laboratory. Isotopic analysis of the LP-3 material by mass spectrometry gave the following results:

Th-232	96.3%
Th-230	0.03%
Th-229	3.66%
Th-228	0.01%

Peaks at 233, 234, and 237 were also detected. Mass spectrometric values on LP-4, the 7-mg remainder of the 10.87 mg total, are not yet available.

In order to obtain a larger quantity of thorium-229 per batch, the extraction equipment had been doubled in size, to 1000 ml capacity, increasing its extraction capacity to a maximum of 200 g of uranium-233. Problems with the extraction steps during this reporting period have been attributed to this increase in volume, although some of the problems, since they were not apparent during the processing of high-purity material, may be partially due to the higher impurity level in the "cow" currently being processed. The problems appeared to be poor contacting of the phases, and lower rates of removal and stripping of uranium-233. To compensate, a larger volume of strip had to be concentrated. Evaluations of the effect of equipment size on extraction efficiency are under way.

A General Plant Project was approved with the objective of keeping the uranium-233 in a liquid state at all times. By eliminating the dissolution, concentration, and ignition-to-the-oxide steps and by eliminating the manual transfer of uranium-233 to and from solid storage containers, it should be possible to nearly double the production rate.
(Ronald L. Deaton and Martin R. Hertz)

URANIUM-234

Mound Laboratory has been separating and recovering high isotopic purity uranium-234 from aged plutonium-238 materials for several years. The general chemical procedures have been described previously.[30]

Final purification of uranium-234, product A15-1, was described in the last report.[31] Calcination and analysis of this product have now been completed. Oxide weight of the final product was 27.818 g. Results of alpha pulse height analysis (6/12/76) and mass analysis of product A15-1 are listed below. Impurities detected by emission spectroscopy included boron, silicon, iron, magnesium,

*An odorless insecticide base from Amsco Solvents and Chemicals Co.

Alpha Pulse Height Analysis	Mass Analysis (wt %)
U-234 = 92.28%	Mass 234 = 95.972
U-232 = 6.43% (21 ppm)	Mass 235 = 0.102
Pu-238 = 0.59% (2.3 ppm)	Mass 236 = 0.045
Other = 0.70% (U-232 daughters)	Mass 238 = 3.818 (some mass 237 observed)

lead, manganese, chromium, gallium, nickel, aluminum, calcium, copper, and silver. Total impurities were estimated to be 1.35% of the oxide, with silicon being the major impurity at 1.15%. Total heat value of the product was determined by calorimetry.

The weight of uranium-234 in product A15-1 was 21.706 g, as calculated from alpha pulse height data and total heat value. Based on mass data and oxide weight corrected for impurities, the uranium-234 content was calculated as 22.292 g. Using the more conservative calculation of 21.706 g, a shipment of 20.100 g of uranium-234 (i.e., 25.758 g of oxide) from product A15-1 was made to Isotope Sales at ORNL on June 21, 1976. The remaining 1.606 g of this product is being held for reprocessing with other material from batch A15.

The preparation of recovered material from the initial processing of product A13-2 for recycle through the final purification was described previously.[32] Two solutions containing approximately 5.6 and 1.9 g, respectively, had been prepared. For a final purification run with each of the two solutions, the uranyl chloride solution was loaded onto a column of Dowex 1 x 4 anion exchange resin (chloride form). Plutonium was eluted with 9M HCl, which contained 0.05M NH_4I as a reductant for the plutonium, and the column was washed with 9M HCl. Neptunium-237 was eluted with 4M HCl, and the uranium-234 was eluted with 0.5M HCl. Analyses indicated 5.5 g of uranium-234 with about one ppm plutonium-238 in the uranium fraction from the first run, and 2.5 g of uranium-234 with about 20 ppm plutonium-238 in the uranium fraction from the second run. The uranium fraction from the second run was held for reprocessing, since the plutonium level was higher than desired. The uranium in the uranium fraction from the first run was precipitated with NH_4OH, calcined to an oxide weight of 6.678 g, and designated product A13-3.

Alpha Pulse Height Analysis	Mass Analysis (wt %)
U-234 = 90.77%	Mass 234 = 99.08
U-232 = 7.11% (23 ppm)	Mass 235 = 0.068
Pu-238 = 0.28% (1.1 ppm)	Mass 236 = 0.053
Other = 1.84% (U-232 daughters)	Mass 238 = 0.798 (some mass 237 observed)

Results of alpha pulse height analysis (8/26/76) and mass analysis on product A13-3 are listed above. Impurities detected in product A13-3 by emission spectroscopy included beryllium, boron, silicon, iron, lead, manganese, magnesium, nickel, aluminum, copper, silver, and calcium. Total impurities were estimated to be 0.39% of the oxide. Total heat value of the product was determined by calorimetry.

The weight of the uranium-234 in product A13-3 was 5.552 g, as calculated from alpha pulse height data and total heat value. Based on mass data and oxide weight corrected for impurities, the uranium-234 content was calculated as 5.574 g. Based on the more conservative calculation of 5.552 g, a shipment of 5.056 g of uranium-234 (i.e., 6.082 g of oxide) from product A13-3 was made to Isotope Sales at ORNL on October 23, 1976. The remaining 0.494 g of this product are being held for reprocessing.

The initial separation of uranium from plutonium "cow" B14-02, which contains 36.6 g of plutonium-238, was completed. This was the third cycle of separation for B14-02, the previous separation having been made about 3-1/2 years ago. This will provide about one gram of very high purity uranium-234 for FY-1977 production. The plutonium "cow" was dissolved in hot, concentrated HNO_3. The solution was divided into two equal parts and adjusted to 2M HNO_3 with NH_4OH. The plutonium in each part was precipitated as the oxalate by a homogeneous precipitation with dimethyloxalate. The oxalate precipitates were collected by vacuum filtration, and calcined to the oxide at 673-773 K (400-500°C) for return to plutonium "cow" storage. The uranium-rich filtrate is ready to be prepared for intermediate separation.
(Perle L. Keister)

CHLORINE ISOTOPE SEPARATION

Chlorine isotopes are being separated by liquid phase thermal diffusion of chlorobenzene in an experimental cascade of 15 columns. Previous reports described early experiments dealing with the relative merits of 1-chloropropane and chlorobenzene as working fluids. Chlorobenzene had been found to be a better fluid from the standpoint of materials compatibility; a full-scale separation experiment using chlorobenzene was started in February 1976. The desired goal of 95% chlorine-35 had been achieved at the time the last report was prepared; however, it had not been possible to reach chlorine-37 concentrations above 87%.

The failure of the chlorine-37 section of the cascade to perform according to theory was attributed to poor performance of the individual thermal diffusion columns near the end of the cascade. Accordingly, six of the last seven columns were isolated for a series of measurements of their performance at total reflux. The columns were emptied, refilled with chlorobenzene of natural isotopic abundance, and restarted. Samples were taken after five and twelve days of operation, and the resulting separations are given in Table 3. The separations are reported in terms of the separation factor, q, defined by:

$$q = \frac{w_{1B}\,(1-w_{1T})}{w_{1T}\,(1-w_{1B})}, \qquad (1)$$

where w_1 is the mass fraction of chlorine-37 and the subscripts B and T refer to the bottom and top of the column, respectively. The values expected for each column, which are also given in the table, are based on the results of earlier research with 60-cm columns.

Of the six columns, only PC8A was found to have an adequate separation factor at total reflux. The remaining columns exhibited varying degrees of poor performance, down to approximately 25% of that expected. Experience suggested that the poor performance was related to nonuniform distribution of temperature on the cold wall of the column. It had previously been possible to gain large increases in column efficiency by reducing cooling water flow rates to values well within the laminar flow region. The resulting elimination of heat transfer by turbulent conduction was believed to have resulted in a much more uniform flow of heat from the cold wall, hence, a more uniform cold wall temperature.

The cooling water flow rate for the measurements reported in Table 3 was such that Re, the Reynolds number, was approximately 1000. Transition from turbulent

Table 3

EQUILIBRIUM SEPARATION FACTORS FOR COLUMNS IN THE CHLOROBENZENE LIQUID THERMAL DIFFUSION CASCADE

Column	Type	Cooling Water Flow Rate (liters/min)	ln q, Measured	ln q, Theor.
SC2B	E	3.5	0.144	0.6
PC8A	C	4.4	0.853	0.76
PC10D	D	4.4	0.178	0.6
PC6A	C	4.4	0.438	0.76
PC8B	C	4.4	0.230	0.76
PC7A	C	4.4	0.294	0.76

to laminar flow in the annular cooling water jacket is presumed to occur at approximately Re = 2000. It would seem that further reduction of the flow rate would have no effect on the mechanism of heat transfer from the cold wall or on the radial temperature distribution; thus, no advantage would be gained from a lower flow rate.

Additional experimentation with columns PC8B and PC7A (type C) showed this presumption to be false. The results of three sets of measurements are given in Table 4. The first set, transcribed from Table 3, corresponds to the original coolant flow rate of 4.4 liters/min; the second, to half of the original flow. The third was taken after thorough cleaning and flushing of the flow distributors and after some minor rearrangements of the inlet piping.

Table 4

PRELIMINARY MEASUREMENTS OF COOLANT FLOW EFFECT

Coolant Flow (liters/min)	ln q	
	Column PC8B	Column PC7A
4.4, original measurement	0.230	0.294
2.2	0.405	0.626
2.2, after flushing and cleaning	0.651	0.780

On the basis of the large increase in separation observed in these experiments, the lower section of the chlorobenzene cascade was reassembled, filled with partially enriched material, and restarted with cooling water flow rates reduced to half of the previous rates. Figure 12 depicts the configuration of the cascade at the time it was restarted. Dimensions of the six types of columns that comprise the system are given in Table 5.

Shortly after the lower section was put back into operation the concentration of chlorine-37 reached the desired value of 90%. Withdrawal of product was started immediately at a rate equivalent to approximately 0.5 g of chlorine-37 per week. Total production during the period June 24 to October 20, 1976, amounted to 5.4 g of chlorine-37 at an average concentration of slightly more than 90%. In the meantime, withdrawal of enriched chlorine-35 from the top of the cascade continued

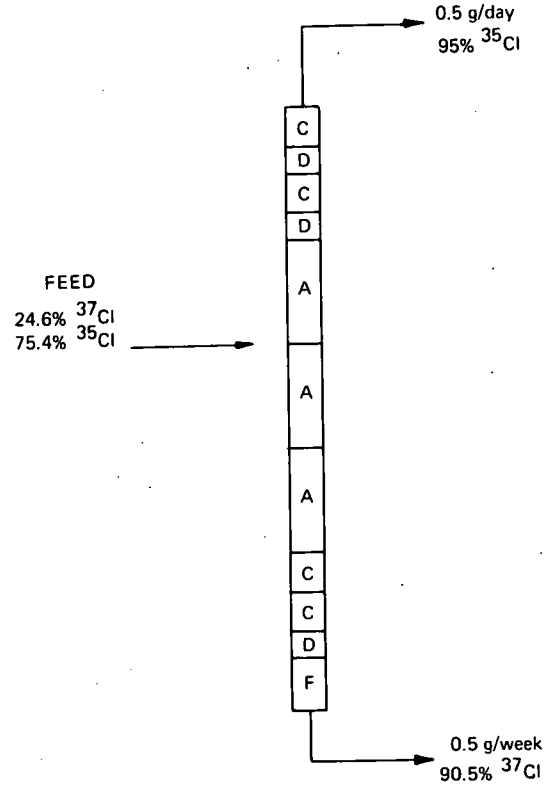

FIGURE 12 - Chlorobenzene liquid thermal diffusion cascade for separating chlorine-35 and chlorine-37. The type of each column is indicated by the letter code; the length of each column is shown proportionately.

Table 5

CHARACTERISTICS OF LIQUID THERMAL DIFFUSION COLUMNS USED IN THE 15-COLUMN CHLOROBENZENE CASCADE

Column Type	Length (m)	Spacing (μm)	Annular Diameter (mm)
A	2.4	300	25
C	0.76	250	25
D	0.6	250	25
F	0.9	180	19
G	0.76	180	19
H	0.76	200	19

at a steady rate equivalent to 0.5 g of chlorine-35 per day. Total production on September 22 amounted to 23.9 g of chlorine-35 at 95% enrichment and 14.0 g at 90% enrichment. Earlier experiments with 1-chloropropane had yielded 10.6 g of chlorine-35 at 90% enrichment.

On September 22 the columns used for chlorine-35 enrichment were rearranged to augment chlorine-37 production, and the separation of highly enriched chlorine-35 was stopped. One type A column was installed as a stripper, and the remaining columns were used to form two parallel chlorine-37 cascades. The present (December 1976) configuration of the system is shown in Figure 13. The left cascade in Figure 13 is the original chlorine-35 section.

Figure 14 shows the concentration profiles in the two sections. The left cascade sustained a major loss of fluid through a leak in late October 1976; consequently, the product concentration is somewhat below the desired value. The right cascade is still accumulating the operating holdup of chlorine-37; thus, concentrations are lower than those in the left cascade. Flat sections in the profile of the left cascade suggest that some of the columns are not performing properly. This is now being investigated.

An estimate of the ultimate production rate of chlorine-37 from this system can be obtained from the flow rate and composition of the depleted stream. Thus,

$$P = (w_F - w_S)\, W \qquad (2)$$

where P is the production rate of chlorine-37, W is the flow rate of the depleted stream, w_F is the weight fraction of chlorine-37 in the feed, and w_S is the weight fraction of chlorine-37 in the depleted stream. From this equation and the data given in Figure 13 a steady state production rate of approximately 0.2 g of chlorine-37 per day is predicted.

Evaluation of Column Parameters One type D column (PC10D) and one type E column (SC2B), identified as having exceptionally poor characteristics, were removed from the cascade for further evaluation. Each column was installed in a test loop similar to the one shown schematically in Figure 15. In each loop the column was connected to a large reservoir of chlorobenzene feed material circulated continuously across the top.

The concentration of chlorine-37 at the bottom of each column was measured as a function of time at a series of cooling water flow rates up to nearly 5 liters/min. Some typical experimental results are plotted in Figure 16. At the conclusion of each experiment the concentration of chlorine-37 in the top reservoir was measured; then the fluid in the system was remixed to a uniform concentration

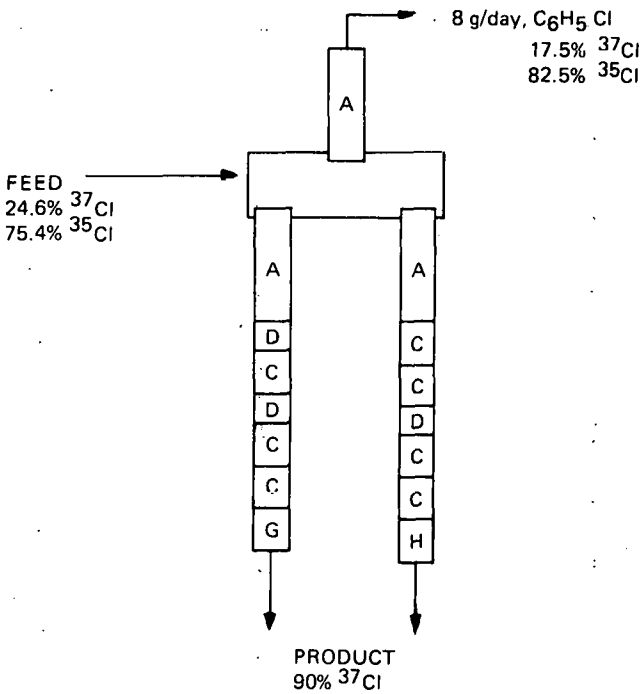

FIGURE 13 - Present configuration of the chlorobenzene liquid thermal diffusion cascade. The type of each column is indicated by the letter code; the length of each column is shown proportionately.

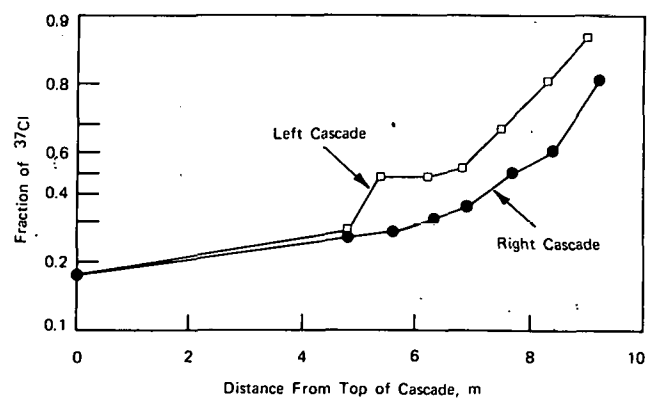

FIGURE 14 - Compositions in the dual liquid diffusion cascade for chlorine-37 enrichment.

by circulating liquid from the top to the bottom of the column and through the reservoir. For some of the experiments with column PC10D a circulating pump was added to the bottom of the column to provide additional holdup, thus extending the time scale of the experiment.

Column coefficients were derived from the measurements by adjusting parameters to fit the solution of the thermal diffusion column transport equation pertaining to the boundary conditions of the experiments. The differential equation which describes the behavior of the column separating a binary mixture is:

$$\mu \frac{\partial w_1}{\partial t} = H(2w_1 - 1) \frac{\partial w_1}{\partial z} + K \frac{\partial^2 w_1}{\partial z^2} \qquad (3)$$

where w_1 is the mass fraction of component 1 (chlorine-37); μ is the holdup per unit length; H is the initial transport coefficient; K is the remixing coefficient; z is the vertical coordinate; and t is the time.

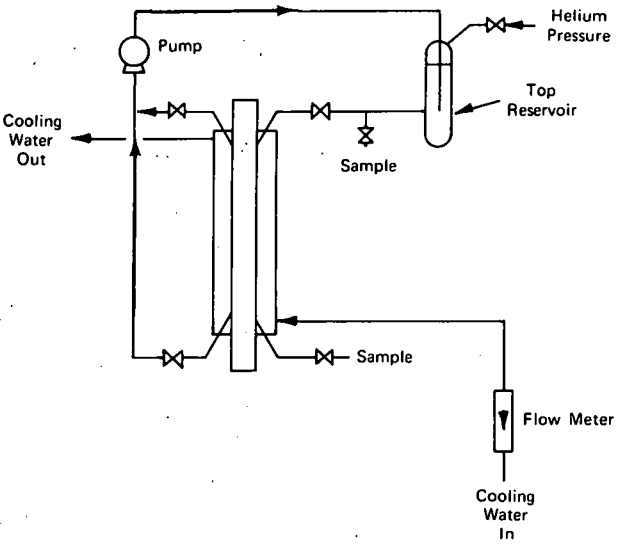

FIGURE 15 - Schematic of system used for column testing.

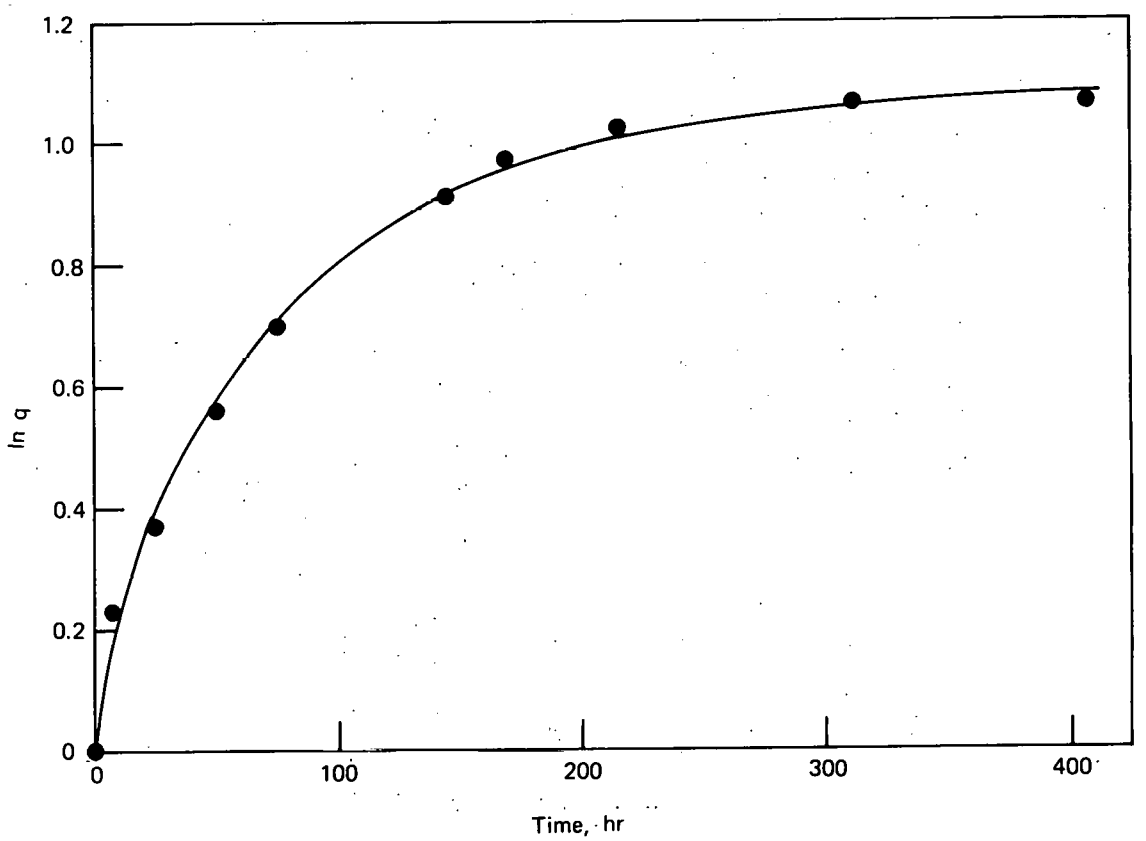

FIGURE 16 - Separation in column PC10D at a water flow rate of 1.4 liters/min.

Eq. 3 can be transformed to:

$$\frac{W}{Y}\frac{\partial w_1}{\partial \theta} = (2w_1-1)\frac{\partial w_1}{\partial y} + \frac{\partial^2 w_1}{\partial y^2} \qquad (4)$$

where W is the total holdup in the column and θ, y, and Y are defined by:

$$\theta = Ht, \qquad (5)$$

$$y = \frac{Hz}{K} \qquad (6)$$

and

$$Y = \frac{HL}{K} \qquad (7)$$

where L is the length of the column.

Existing computer programs were used to solve Eq. 4 as a function of θ for a series of ten values of Y. A simplex optimization routine was then used to select the values of H and Y which resulted in the best fit of an interpolated theoretical curve to the experimental separation data. The fit was based on the minimization of the quantity d, according to the following equation:

$$d = \sum_{i=1}^{n} (\ln q_{xi} - \ln q_{ti})^2 \qquad (8)$$

where q_{xi} and q_{ti} are the experimental and theoretical separation factors for the i^{th} experimental time value. The values of q_{ti} were obtained by double table lookup and parabolic interpolation of the numerical solutions of Eq. 4.

The resulting column parameters are plotted in Figures 17 and 18 as a function of water flow rate. A striking feature of both plots is the large increase in Y as the water flow is reduced. In both cases the expected value of 0.6 is exceeded. An equally striking feature is the fact that H, the initial transport coefficient, increases with decreasing water flow for column PC10D, whereas the opposite behavior is observed for column SC2B.

The remixing coefficient, K, calculated from Eq. 7 and from the experimental parameters H and Y, is also plotted in Figures 17 and 18. The remixing coefficient for column PC10D is affected only slightly by water flow; however, a large increase is observed for SC2B at high flow rates. The increase is most likely the result of a parasitic circulation which is suppressed by the vertical temperature gradient imposed on the column by low rates of coolant flow. (The temperature increase of the water is plotted in Figures 17 and 18 for reference.)

There does not appear to be a parasitic contribution to the remixing coefficient for PC10D. In fact a rough calculation of K from theory gives a value of about 0.002 g cm/sec -- somewhat higher than all of the experimentally derived values. A tentative conclusion is that there are two effects associated with the variation in water flow. The first, and dominant one in the case of SC2B, is a suppression of parasitic circulation by an imposed vertical temperature gradient. The second effect is most readily apparent for PC10D; however, it may also be marginally evident at low flow rates for SC2B. The second effect is characterized by the covariant increase of H and Y as water flow is reduced. There does not seem to be any satisfactory explanation for this behavior other than a possible, but very unlikely, large effect of temperature on the isotopic thermal diffusion factor. *(William M. Rutherford)*

MOLECULAR BEAM SCATTERING

Initial testing of the molecular beam quadrupole detector system was completed. The desired sensitivity (1.0×10^{-4} beam fraction) has been obtained using the lock-in amplifier technique. Signal averaging by computer program was incorporated with good results. The signal averaging technique can retrieve the signal at the same level as the lock-in amplifier, but with a potential for one or two orders of magnitude improvement. Detector measurements have thus far been made using reduced single beam intensity scaling by source pressure control. The beam fraction of 1.0×10^{-4} is the lowest which can be accurately obtained by this method. The limit of detector sensitivity will be determined after the second arm of the beam chamber has been outfitted with its source. The lower level scattered intensity, produced from crossed beam collisions, will then be obtained.

The nozzle-skimmer source for the second arm of the molecular beam chamber has been assembled, aligned, and leak tested satisfactorily. This source is the twin to the one currently being used in the primary-beam arm which has been described in detail.[33] The same Cryotip refrigeration system will be used for cooling both sources. The new source is currently being installed in the chamber, and the secondary beam forming components are

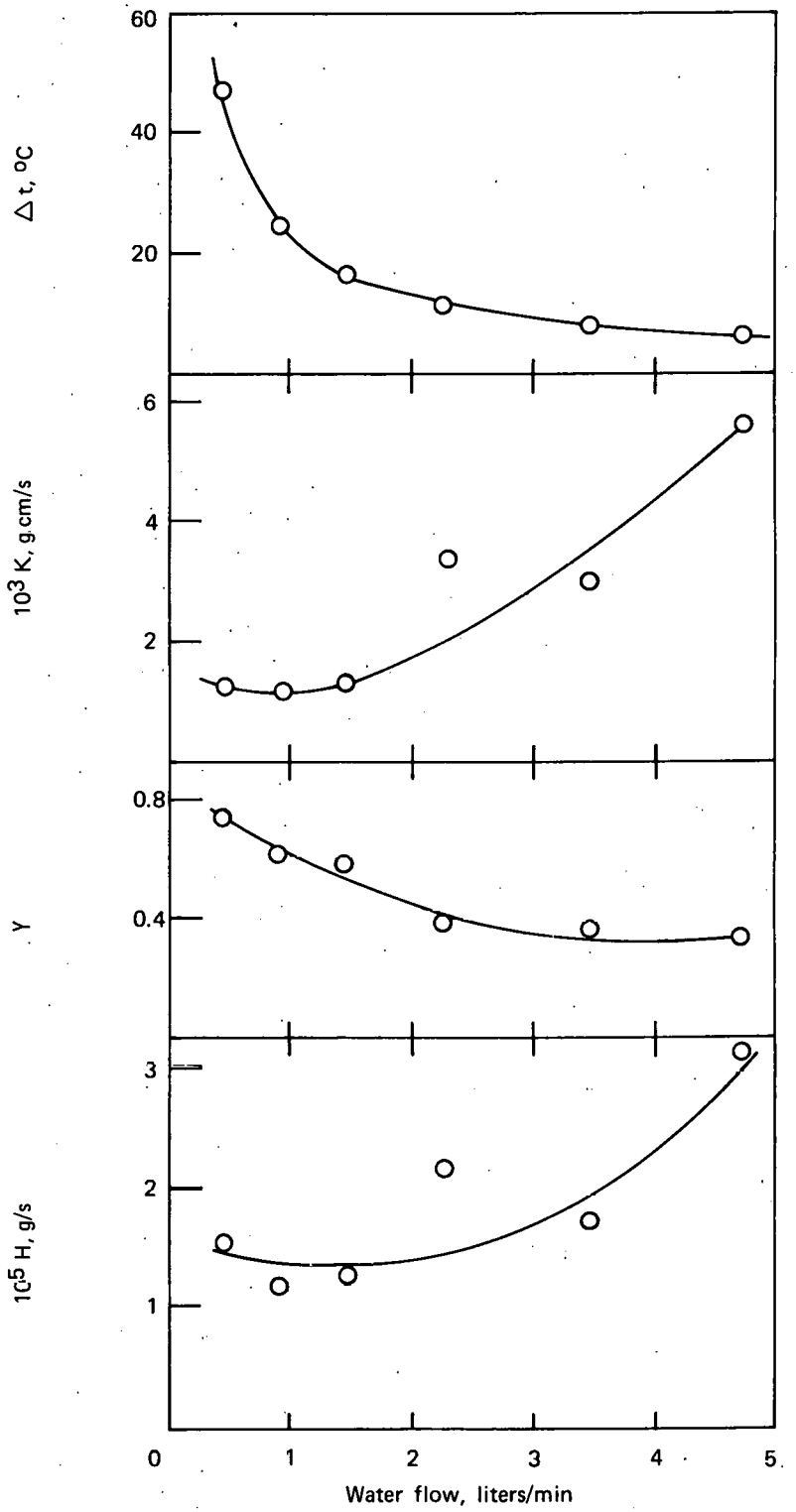

FIGURE 17 - Experimental parameters for columns SC2B.

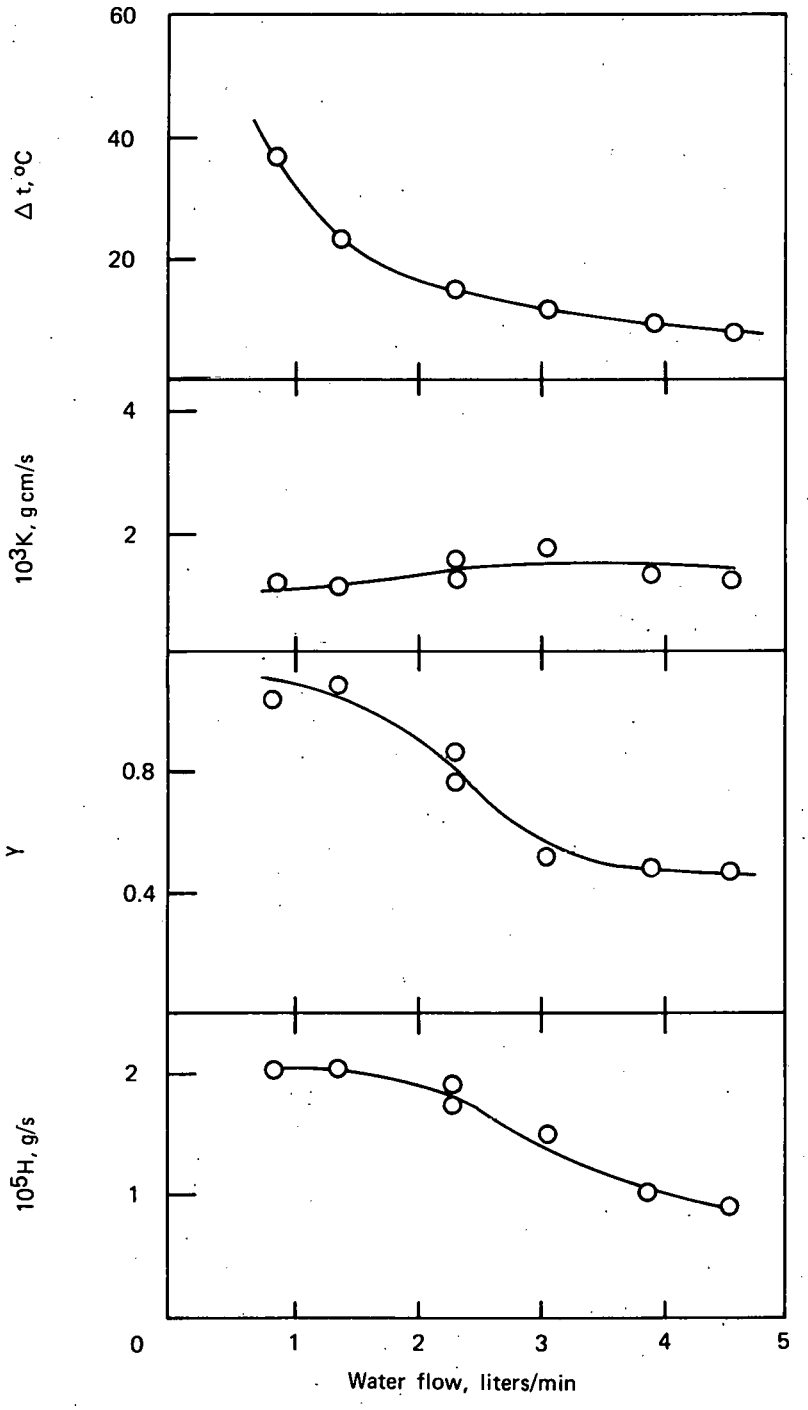

FIGURE 18 - Experimental parameters for column PC10D.

being aligned to give the crossed beam differential scattering capability mentioned above.

A new cryogenically cooled target gas cell was designed and fabricated. This new cell will permit greater precision in the position adjustment of the target orifice, and will have the capability for low temperature operation through the use of a Cryotip refrigeration system similar to that used on the sources. This low temperature capability will greatly increase the relative velocity range over which total cross sections can be measured. The new cell is scheduled to be installed in the primary-beam arm of the chamber during the first quarter of CY-1977.

Work has begun on the design and construction of a drive mounting system for one of the velocity selector rotors which were fabricated some time ago. This rotor design was described in an earlier report.[34] The addition of velocity selection will give a nearly monoenergetic primary beam and the capability for accurate velocity distribution measurements for nozzle beams. Knowledge of this distribution will allow cross-sectional measurements of differential scattering to be accurately corrected for relative velocity spread. Fabrication and testing of the velocity selector are scheduled to be completed by late summer 1977.

The results of the argon-krypton total cross section experiments described previously[35] were reported in a paper entitled "Low Energy Total Cross Sections for the Argon-Krypton System" presented at the Tenth International Symposium on Rarefied Gas Dynamics (July 18-24) in Aspen, Colorado. The presentation was well received and evoked several good questions. Since the symposium, the manuscript has been accepted for publication by the American Institute of Aeronautics and Astronautics, New York, in January 1977. *(Robert W. York)*

TRANSPORT PROPERTIES

Thermal Diffusion Factors for ^{3}He-^{4}He

The experimental low-temperature thermal diffusion factors for the ^{3}He-^{4}He system, which were measured in the two-bulb apparatus at this laboratory several years ago, have been re-evaluated. The need for such an evaluation arose because subsequent data taken at low temperatures in a seven-tube trennschaukel[36,37,38] indicate a behavior somewhat at variance with the two-bulb results. The trennschaukel results showed α_T increasing gradually with decreasing temperature from ~0.068 at 250 K to a broad flat maximum at ~0.08 in the region from 3 to 30 K. Below 3 K, α_T dropped rather rapidly. On the contrary, a thermal diffusion factor of ~0.1 appeared to be increasing at 4.2 K based on the admittedly incomplete two-bulb data.[39,40] The nature of the van der Waals forces in the helium interaction should be sensitively reflected in the behavior of α_T at very low temperatures, and it is thus important to have reliable and accurate experimental thermal diffusion factors in this temperature region.

A fundamental difference exists between the two experimental methods. With the trennschaukel the entire experiment is conducted with the apparatus and gas at very nearly the assigned temperature for α_T. Thus for α_T at 3 K, the hot and cold blocks may be held at 3.2 and 2.8 K, respectively, during the course of the experiment. A value of α_T is obtained from the isotopic separation obtained in the device. (See Reference 36 for a detailed discussion of trennschaukel design and operation.) In the case of the two-bulb apparatus, the hot region is held at a fixed temperature, in this case 300 K, and the cold temperature is varied. From a series of experiments, α_T is obtained from the slope of the logarithmic plot of T_H/T_C vs the separation factor. The pitfall of this method is that the numerical value of α_T is very sensitive to the derivative of the curve of unspecified functional form which must be fitted to the experimental points, each of which in turn has uncertainties in $\ln q$ and $\ln T_H/T_C$ associated with it. The problem is particularly severe at the end points of the curve.

With the foregoing arguments in mind, it was deemed advisable to comprehensively analyze the previous two-bulb work, examining the following: a) experimental apparatus; b) applicability of existing theory to the experimental conditions; and c) estimated experimental uncertainties and interpretation of the data.

a) Apparatus

The apparatus shown in Figure 19 was constructed by Dr. Stanley Weissman for measuring thermal diffusion factors between 4.2 and approximately 77 K. It is known as the "new" apparatus because Dr. Weissman had, prior to 1970, measured and published experimental results down to 55 K in a different "old" apparatus.[41]

The lower chamber, A, is connected to the upper portion of the apparatus by tube, D, through a stopcock, K. Above this

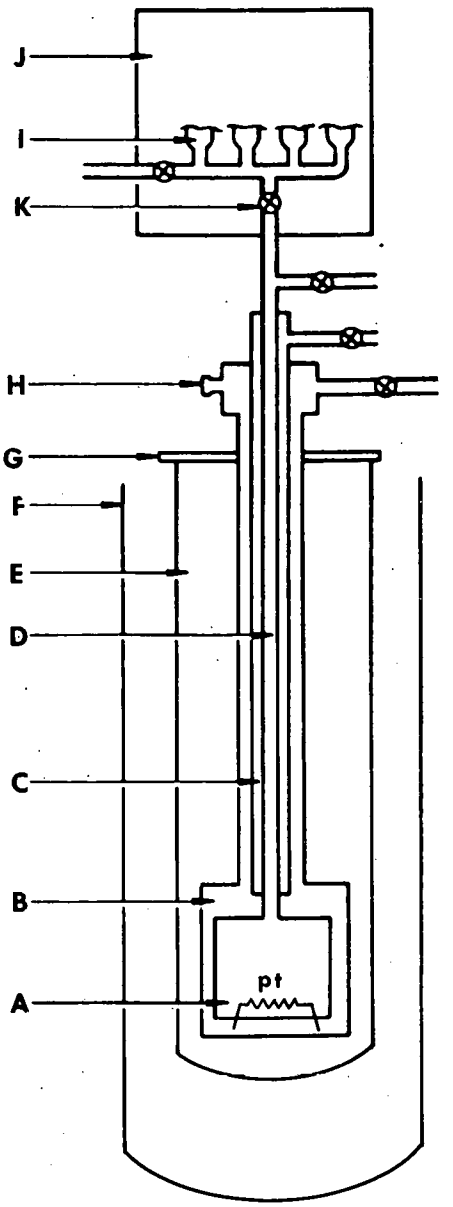

FIGURE 19 - Two-bulb apparatus. A, lower chamber; B, exchange gas space; C, vacuum jacket; D, connecting tube; E, inner dewar; F, outer dewar; G, flange; H, electric feed-through; I, one of four female tapers; J, water bath; K, connecting tube stopcock; and Pt, platinum resistor.

stopcock is the volume which makes up the hot chamber of the two-bulb cell. This volume is made up, in part, by four metal female tapers denoted by I, into which sample bottles can be placed. The entire upper chamber and both stopcocks are located in a thermostated water bath, J. Since this part of the apparatus is always isothermal, the gas contained in it has uniform composition.

The temperature of the lower chamber is maintained by sensing the gas temperature with a platinum resistance thermometer standing on its platinum leads in A, which in turn pass through the chamber wall by means of a ceramic-to-metal seal. This controls a heater around A by means of a bridge circuit. An analysis of the experimental apparatus showed that good vacuum and cryogenic techniques were followed with one possible exception: the use of a platinum resistance thermometer, and its suspension in the gas, for use at very low temperatures. Below about 15 K the resistance of the platinum thermometer falls to only a few tenths of an ohm and the bridge control becomes rather insensitive. Also the heat generated by the bridge current in the resistor, if not conducted out through the leads, may locally heat the surrounding gas leading to an error in T_C. A second platinum resistor and a 10Ω Allen-Bradley carbon resistor were therefore embedded in the copper base of A so that any one of the three resistors could be used in the bridge circuit to control the heater current and hence, the temperature of A.

The carbon resistor was calibrated independently of the platinum resistors by using the triple point of neon and the vapor pressure of helium-4 with liquid in A. The control of T_C with the calibrated carbon resistor, as well as the accuracy with which T_C can be measured, is far superior below 25 K than with the original platinum resistor. Above 25 K the platinum resistor in the block can be used for control without fear of dissipating I^2R heat losses into the gas. While it was originally thought that self-heating of the original resistor may have introduced serious errors into the measurement, comparative readings above 25 K showed discrepancies of up to $\Delta = 2$ K, which introduces some uncertainty, but not of a serious nature. On the other hand, the lack of sensitivity in either platinum resistor below 25 K is a serious problem.

b) Applicability of Theory to the Experiments

The theory of the thermal diffusion process in the two-bulb apparatus has been treated several times in the literature, but the most rigorous treatment is by Lonsdale and Mason.[42] Unfortunately, Lonsdale and Mason used radioactive tracers in their work and their derivation of the working equations is not strictly applicable to Weissman's case of equimolar mixtures. In Reference 41, Weissman made several simplifying assumptions to arrive at Eq. 4, which unfortunately was printed incorrectly in the manuscript. The restriction of one component present in trace amounts, and the simplifying assumptions used by Weissman are removed in the following derivation which uses in large part the logic of Lonsdale and Mason.

The thermal diffusion factor is determined from:

$$\alpha_T = \frac{d \ln q}{d \ln (T_H/T_C)},$$

where T_H = constant and thus α_T at any temperature, T_C, is the slope of ln q vs ln (T_H/T_C) at the point corresponding to T_C.

In the present apparatus only ${}^3X_H$ of mass 3 need be (or can be) measured, so it is necessary to derive the value of ${}^3X_C$ at the end of the experiment in order to obtain the separation factor, q. The superscript "3" can be dropped and henceforth X(t) will define the mole fraction of ^{3}He, initially at t = 0 and at t = ∞, when the steady state is achieved.

$$q \equiv \frac{X_H(\infty)}{1-X_H(\infty)} \Big/ \frac{X_C(\infty)}{1-X_C(\infty)}$$

This is the separation factor for non-trace mixtures and does not contain that approximation used in defining q in Reference 42. $X_C(\infty)$ is derived in terms of: $X_{Feed} = X(0)$; $X_H(\infty)$; the dimensions of the apparatus; and the temperatures in the experiment.

At time t = 0, there are:
$n_C(0)$ atoms of mass 3 in V_C at T_C;
$n_H(0)$ atoms of mass 3 in V_H at T_H; and
$n_L(0)$ atoms of mass 3 in the connecting tube of area, A, and length, L.

At time t = ∞ (steady state), there are:
$n_C(\infty)$ atoms of mass 3 in V_C at T_C;
$n_H(\infty)$ atoms of mass 3 in V_H at T_H; and
$n_L(\infty)$ atoms of mass 3 in the connecting tube.

The total number of atoms is constant in time, e.g.,
$n_C(0) + n_H(0) + n_L(0) = n_C(\infty) + n_H(\infty) + n_L(\infty)$,
or $n_C(\infty) - n_C(0) = -[n_H(\infty) - n_H(0)] - [n_L(\infty) - n_L(0)]$.

In terms of concentration changes, this is $\Delta n_C = \Delta n_H - \Delta n_L$.

Defining N as the total number of atoms, we have:

$$\frac{X_H(\infty)}{X_C(\infty)} = \frac{n_H(\infty)/N_H(\infty)}{n_C(\infty)/N_C(\infty)} = \left[\frac{n_H(0) + \Delta n_H}{n_C(0) - \Delta n_H - \Delta n_L}\right]\frac{N_C(\infty)}{N_H(\infty)}$$

The pressure and total volume are constant everywhere and at all times, hence the total molecular density is constant.

$$N_H(0) = N_H(\infty) = N_H \text{ and } N_C(0) = N_C(\infty) = N_C$$

Furthermore, since $\Delta X_H = \Delta n_H/N_H$, and $X_H(0) = X_C(0)$, and using:

$$n_H(0)/N_H(\infty) = n_H(0)/N_H = X_H(0);$$

$$\Delta n_H/N_H(\infty) = \Delta n_H/N_H = \Delta X_H;$$

$$n_C(0)/N_C(\infty) = n_C(0)/N_C = X_C(0) = X_H(0);$$

$$\Delta n_H/N_C(\infty) = \Delta X_H\, N_H/N_C; \text{ and}$$

$$\Delta n_L/N_L(\infty) = \Delta n_L/N_C;$$

we obtain

$$\frac{X_H(\infty)}{X_C(\infty)} = \frac{X_H(0) + \Delta X_H}{X_H(0) - \Delta X_H\frac{N_H}{N_C} - \frac{\Delta n_L}{N_C}}$$

Assume the ideal gas law holds, i.e.,

$$N_C = PV_C N_O/RT_C \text{ and } N_H = PV_H N_O/RT_H,$$

where N_O = Avogadro's number. Then $N_H/N_C = V_H T_C/V_C T_H$. Substituting this into the equation above, dividing through by $X_H(0)$, using $\Delta X_H = X_H(\infty) - X_H(0)$ and inverting gives the equation:

$$\frac{X_C(\infty)}{X_H(\infty)} = \frac{X_H(0)}{X_H(\infty)}\left\{1 - \frac{V_H T_C}{V_C T_H}\left[\frac{X_H(\infty)}{X_H(0)} - 1\right] - \frac{\Delta n_L}{X_H(0) N_C}\right\}$$

The explicit expression for the composition in the cold bulb at the end of the experiment is:

$$X_C(\infty) = X_F + \frac{V_H T_C}{V_C T_H}\left[X_F - X_H(\infty)\right] - \frac{\Delta n_L}{N_C}$$

This expression does not agree with Eq. 4 in Reference 41 but it apparently was used by Weissman in calculating numerical values. Eq. 4 in Reference 41 is therefore assumed to be a typographical error.

It remains to determine an expression in known quantities for $\Delta n_L/N_C$, which is the correction for the finite volume of the connecting tube. At this point the assumptions that the composition and temperature in the connecting tube are simply arithmetic averages of the respective quantities in the hot and cold bulbs are dropped. Then:

$$\Delta n_L = n_L(\infty) - n_L(0),$$

where $n_L(0) = N_L X_H(0) = N_L X_F$, and

$$n_L(\infty) = \int_{Z=0}^{Z=L} dn_L(\infty, Z)$$

The differential $dn_L(\infty,Z)$ represents the composition gradient at the steady state due to the temperature gradient along the connecting tube. The variable Z stands for any point on the connecting tube. Since AdZ = dv, the quantity N_L is evaluated as follows:

$$N_L = \int_{Z=0}^{Z=L} dN_L(Z) = \int_0^L \frac{PN_O}{RT}\, dV$$

$$= \int_0^L \frac{PN_O A}{RT(Z)}\, dZ$$

In order to integrate this equation, we must obtain an expression for the temperature gradient. An analysis of the present apparatus and operating conditions shows the temperature gradient in the connecting tube to be determined by heat flow in the gas column and in the tube wall in a ratio of approximately 3:1. A reasonable approximation for the temperature distribution is then that given in Reference 42, i.e.,

$$T(Z) = T_H - \frac{T_H - T_C}{L} Z$$

Now N_L becomes:

$$N_L = \int_0^L dN\,(Z)$$

$$= \int_0^L \frac{PN_O A}{RT(Z)}\, dZ = \frac{PN_O AL}{R(T_H - T_C)} \ln\left(\frac{T_H}{T_C}\right)$$

Also, $n_L(0) = N_L X_F = \frac{PN_O ALX_F}{R(T_H - T_C)} \ln\left(\frac{T_H}{T_C}\right)$

The quantity $n_L(\infty)$ is evaluated as follows:

$$dn_L(\infty,Z) = X_L(\infty,Z)\, dN_L = \frac{X_L(\infty,Z)\, PN_O A\, dZ}{RT(Z)}$$

To find $X_L(\infty,Z)\, dN_L$, we assume a composition distribution for $X_L(\infty,Z)$ given by:

$$\ln \frac{X_H(\infty)/1 - X_H(\infty)}{X_L(\infty,Z)/1 - X_L(\infty,Z)} = \bar{\alpha}_T \ln\left(\frac{T_H}{T(Z)}\right),$$

since $q \equiv \left[\frac{X(\text{light})}{X(\text{heavy})}\right]_{T_H} \Big/ \left[\frac{X(\text{light})}{X(\text{heavy})}\right]_{T_C}$

and $T_L < T_H$.

Here $\bar{\alpha}_T$ is initially an estimated mean value for the temperature range. Solving for $X_L(\infty,Z)$, the following are obtained:

$$\frac{1-X_L(\infty,Z)}{X_L(\infty,Z)} = \frac{1-X_H(\infty)}{X_H(\infty)}\left(\frac{T_H}{T(Z)}\right)^{\bar{\alpha}_T}$$

$$X_L(\infty,Z) = \left[1+\left(\frac{1}{X_H(\infty)}-1\right)\left(\frac{T_H}{T(Z)}\right)^{\bar{\alpha}_T}\right]^{-1}$$

$$dn_L(\infty,Z) = \left[1+\left(\frac{1}{X_H(\infty)}-1\right)\left(\frac{T_H}{T(Z)}\right)^{\bar{\alpha}_T}\right]^{-1}\frac{PN_OAdZ}{RT(Z)}$$

$$n_L(\infty) = \int_0^L dn_L(\infty,Z) = \frac{PN_OA}{R}$$

$$\int_0^L \frac{dZ}{\left[1+\left(\frac{1}{X_H(\infty)}-1\right)\left(\frac{T_H}{T_H-\frac{T_H-T_C}{L}Z}\right)^{\bar{\alpha}_T}\right]\left[T_H-\frac{T_H-T_C}{L}Z\right]}$$

This rather horrendous expression can be analytically integrated by making the change of variable $X = a + bZ$ with the result:

$$n_L(\infty) = \frac{PN_OAL}{R(T_H-T_C)}\ln\left\{(T_H/T_C)\left[X_H(\infty)+[1-X_H(\infty)](T_H/T_C)^{\bar{\alpha}_T}\right]^{-1/\bar{\alpha}_T}\right\},$$

The correction term $\Delta n_L/N_C$ is:

$$\frac{\Delta n_L}{N_C} = \frac{n_L(\infty)-n_L(0)}{N_C}$$

$$= \frac{V_TT_C}{V_C(T_H-T_C)}\ln\left\{(T_H/T_C)^{1-X_F}\left[X_H(\infty)+[1-X_H(\infty)](T_H/T_C)^{\bar{\alpha}_T}\right]^{-1/\bar{\alpha}_T}\right\}$$

since $AL = V_T$. The correction term is now expressed in known quantities and in turn allows $X_C(\infty)$ to be calculated from the experimental conditions and apparatus dimensions. Only one step remains and that is to calculate the thermal diffusion factor, α_T, for the experiment. This, of course, should agree with the mean value, α_T, used in evaluating the correction factor. If it does not, the calculation must be iterated until it is consistent. The value of the separation factor, q, used in the plot of ln q vs ln (T_H/T_C) is that obtained using the self-consistent value of $X_C(\infty)$.

A computer program was written which calculated the derived quantities and performed the necessary iterations to provide self-consistent values of $X_C(\infty)$ and hence q.

c) Estimated Uncertainties and Interpretation of Data

The uncertainty in the determination of the thermal diffusion factor at a specific temperature, from the slope of the ln q vs ln (T_H/T_C), will be dependent upon the accuracy with which each individual experiment is conducted. The approach here will be to compute the uncertainties in individual experiments, assign error bars, and observe graphically how these individual uncertainties can affect the slope determination. The measured experimental quantities are 1) the feed composition, 2) the composition in the hot bulb and 3) the hot and cold bulb temperatures. Each of these quantities has associated with it an inherent experimental uncertainty.

The resultant effect is calculated as follows:

Uncertainty in q: $q \equiv (X_H/1-X_H)/(X_C/1-X_C)$,

where X_C is not measured directly, but is evaluated in terms X_F and X_H by the expression derived previously. Although $\Delta n_L/N_L$ is a function of X_F and X_H, this term is very small and slowly varying. We therefore make the approximation: $X_C \simeq X_F + a(X_F-X_H)$, where $a = V_HT_C/V_CT_H$.

$$\frac{\partial q}{\partial X_F} = -\left(\frac{X_H}{1-X_H}\right)\frac{(1+a)}{[(1+a)X_F-aX_H]^2}$$

$$\frac{\partial q}{\partial X_H} = \frac{[(1+a)X_F-aX_H][1-(1+a)X_F+aX_H]+aX_H(1-X_H)}{\{(1-X_H)[(1+a)X_F-aX_H]\}^2}$$

The percentage of total uncertainty due to composition analysis of feed and hot bulb samples is:

$$dq = \left|\frac{\partial q}{\partial X_F}\right||\Delta X_F| + \left|\frac{\partial q}{\partial X_H}\right||\Delta X_H|,$$

and therefore $\Delta \ln q = dq/q$ and $\%\Delta \ln q = 100\Delta \ln q/\ln q$.

Uncertainty in T: $\frac{\partial (T_H/T_C)}{\partial T_H} = \frac{dT_H}{T_C}$;

$$\frac{\partial (T_H/T_C)}{\partial T_C} = - \frac{T_H dT_C}{T_C^2},$$

$$d(T_H/T_C) = \left|\frac{dT_H}{T_C}\right| + \left| - \frac{T_H dT_C}{T_C^2}\right|$$

so therefore, $\Delta \ln (T_H/T_C) = \left|\frac{\Delta T_H}{T_H}\right| + \left|- \frac{\Delta T_C}{T_C}\right|$

and $\% \Delta \ln (T_H/T_C) = \frac{100 \Delta \ln (T_H/T_C)}{\ln (T_H/T_C)}$.

The estimated uncertainties were evaluated for each experiment. Uncertainties in the mass spectrometric analyses were estimated to be the differences between the duplicate samples as is done in trennschaukel experiments; temperature uncertainties were inferred from entries in the original data. All of the previous experiments are shown in Figure 20. The solid circles were data taken in the "old" apparatus and are plotted as published in Reference 41. The twelve open circles with error bars are the data taken in the "new" apparatus, with q evaluated by means of the revised theory in section b) above, and with the experimental data taken directly from the original laboratory notebook. The error bars were calculated based on estimates made according to the discussion above.

Computed q values in general did not differ appreciably from those reported in Reference 39; this is not surprising in view of the fact that the tube correction term, $\Delta n_L/N_C$, is quite small. The results of one experiment (#40) differed significantly upon recalculation, which probably reflects a computational error; results from a second experiment (#42) were very low and not given in the original compilation. The data are summarized in Table 6. Experiments #40 and 42# are unrealistically low and #37 and #41 appear suspiciously low. The latter two experiments fall into the region where there is undoubtedly a sensitivity problem with the thermometer.

The scatter and estimated uncertainties of the data are such that it is not feasible to obtain an accurate evaluation of the slope. It is the opinion of this writer that the best that can be done is to pass a broad band through the data implying an approximately constant α_T with some relatively great associated uncertainty.

In order to obtain an estimate of the level of sensitivity that would be needed in the experiments to discriminate among intermolecular potentials, a numerical integration procedure was adopted to eliminate the inaccuracies of numerical differentiation of the widely scattered data. This method also provides a directly calculated value of the separation factor as a function of T_C. The procedure used was as follows: theoretical calculations of $[\alpha_T]_3$ were performed at 1° intervals from 1 to 303 K using two different sets of quantum transport collision integrals for helium-3/helium-4. The collision integrals had been computed previously[43,44] using the Beck and Bruch-McGee potentials for helium. The logarithm of the separation factor was obtained as a function of T_C by numerical integration of the computed $[\alpha_T]_3$ values in the following equation:

$$\ln q = \int_{T_C}^{T_H} [\alpha_T]_3 \, d\ln T = \int_{T_C}^{T_H} [\alpha_T]_3/T \, dT$$

The theoretical separation factors for the two potentials are shown by the solid and dashed curves in Figure 20. This calculation demonstrates vividly that the experimental uncertainty and the scatter completely mask the difference in q caused by the potentials. The insert shows the advantage of conducting the experiment below 4.2 K where the difference is magnified. Under the present expectations with regard to temperature control and accuracy of analysis, it will be necessary to conduct experiments at temperatures as low as approximately 2 K in order to discriminate between the two potentials. *(W. L. Taylor)*

Thermal Diffusion Factors for Ar-Xe and Kr-Xe Thermal diffusion factors for the final two binary mixtures of the noble gases, Ar-Xe and Kr-Xe, were measured in the 20-tube trennschaukel. The composition dependence was determined at 250 K and the α_T's for equimolar mixtures were measured as a function of temperature up to 750 K, as was done for other binary noble gas mixtures as reported earlier.[45-48] The experimental results are given in Tables 7 and 8. The composition dependences for the two systems are shown in Figure 21 along with the least squares fit to the data (solid line).

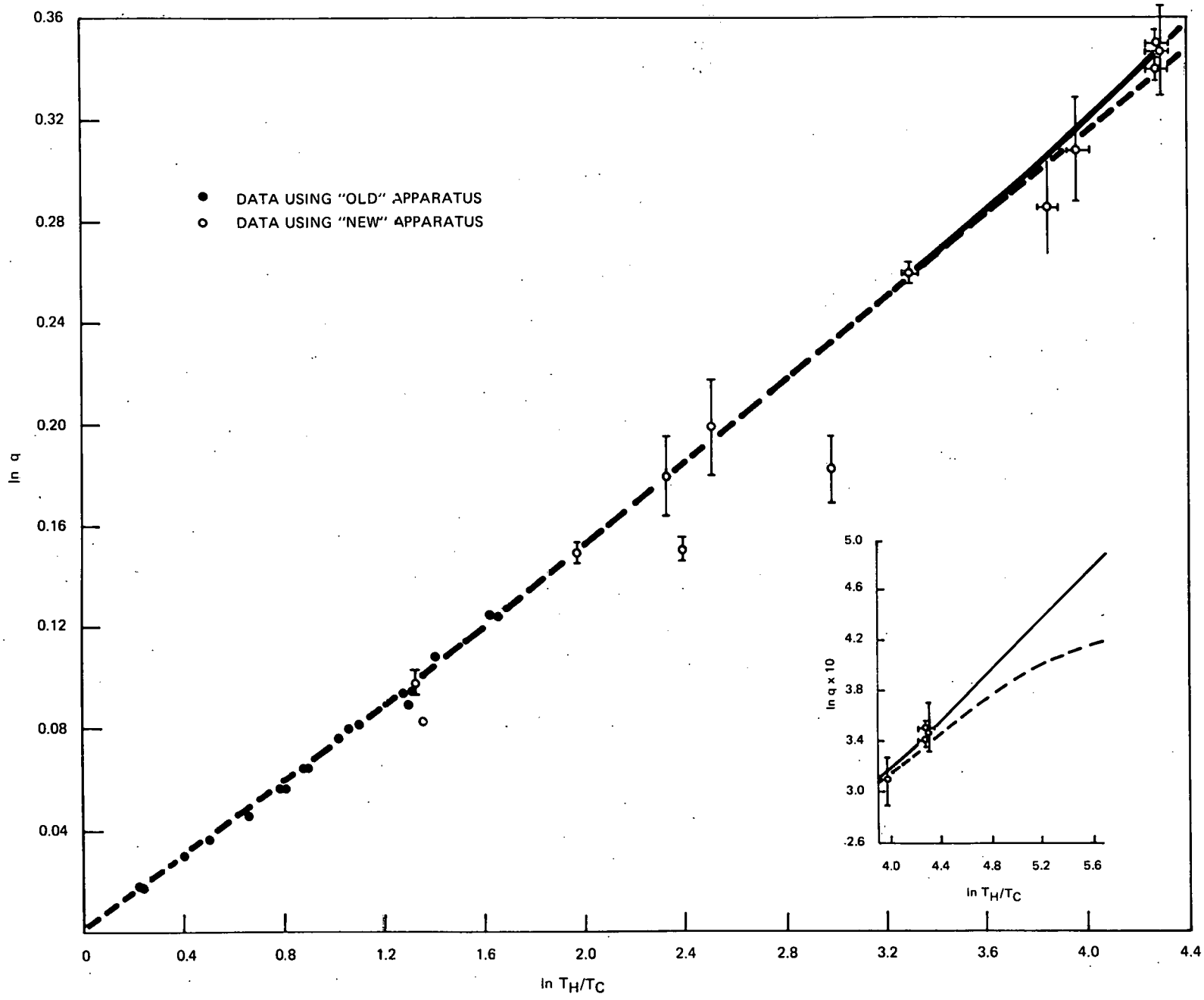

FIGURE 20 - Separation factor (q) for helium-3/helium-4 increases with the temperature ratio (T_H/T_C) in two-bulb experiments. The theoretical curves shown were obtained by numerical integration of theoretical thermal diffusion factors calculated using the Beck (——) and Bruch-McGee (---) potentials for helium.[43,44]

Table 6

THEORETICAL CALCULATIONS OF LOW-TEMPERATURE SEPARATION FACTORS FOR HELIUM-3/HELIUM-4 MEASURED IN "NEW" APPARATUS

Experiment Number	T_C (K)[a]	Approximate Theory ln (T_H/T_C)	Approximate Theory ln q	Rigorous Theory[b] ln q	Rigorous Theory % Uncertainty ln (T_H/T_C)	Rigorous Theory % Uncertainty ln q
29	77.3	1.3668	0.09802	0.09773	0.3	5.1
35	41.0	2.0012	0.14878	0.14911	0.3	3.0
39	28.8	2.3550	0.17213	0.17990	0.4	9.2
40	27.1	2.4158	0.16337	0.15073	0.4	2.9
34	24.3	2.5198	0.20055	0.19935	0.4	9.7
42	14.2	3.0618	not given	0.18233	0.6	7.6
36	11.1	3.3081	0.25953	0.26033	0.7	1.6
37	6.4	3.8581	0.28521	0.28592	1.0	6.4
41	5.7	3.9685	0.31018	0.30890	1.2	6.7
31	4.2	4.2796	0.34024	0.34054	1.1	1.2
32	4.2	4.2796	0.35008	0.35078	1.1	1.2
30	4.2	4.2806	0.34691	0.34761	1.1	5.3

[a] T_H was very nearly 303 K in all cases.

[b] The temperatures and associated deviations were taken from the original data. The effect of lack of sensitivity in the platinum thermometer to T_C will be investigated in future experiments.

The equations for the least squares expressions are given by:

$1/\alpha_T = -8.98X_{Ar} + 20.4$ for Ar-Xe (4.6%)

and

$1/\alpha_T = -5.39X_{Kr} + 54.8$ for Kr-Xe (2.0%).

In each case the percentage in parentheses is the average of the deviation of the experimental points from the least squares equations.

The temperature dependences for the two systems are shown in Figure 22. In both cases excellent agreement was obtained with the earlier determination made using thermal columns.[49] *(W. L. Taylor)*

Table 7

α_T FOR AN EQUIMOLAR MIXTURE OF Ar-Xe

Run No.	T_{AV} (K)	α_T (corr.)	Corrections[a]			Uncertainties[a] (±%)		
			A	B	C	D	E	F
552	351	0.117	0.991	1.038	0.976	2.8	2.5	5.3
548	451	0.160	0.992	1.030	0.969	0.8	2.8	3.6
554	553	0.187	0.995	1.034	0.973	1.8	3.0	4.8
556	653	0.205	0.996	1.036	0.975	2.5	2.8	5.3
550	752	0.223	0.999	1.030	0.970	1.5	4.2	5.7

α_T FOR AN EQUIMOLAR MIXTURE OF Kr-Xe

553	350	0.0374	0.981	1.036	0.976	7.3	1.3	8.6
547	451	0.0590	0.991	1.041	0.979	2.3	2.7	5.0
555	552	0.0689	0.990	1.043	0.980	2.0	2.9	4.8
557	653	0.0796	0.990	1.043	0.980	5.3	2.8	8.1
551	752	0.0891	0.990	1.031	0.971	1.7	4.2	5.9

[a](A) Correction from the exponential approach to equilibrium.
(B) Correction from the disturbance caused by pumping.
(C) Correction from back diffusion in the capillaries.
(D) Uncertainty from composition analysis.
(E) Uncertainty from temperature measurements.
(F) Total uncertainty.

Table 8

α_T FOR THE Ar-Xe SYSTEM AT 250 K

Run No.	X_1[a] (feed)	α_T (corr.)	Corrections[b]			Uncertainties[b] (±%)		
			A	B	C	D	E	F
564	0.098	0.0491	0.983	1.031	0.970	3.8	0.9	4.7
567	0.322	0.0598	0.987	1.042	0.979	4.2	2.2	6.4
561	0.503	0.0648	0.990	1.042	0.979	9.1	0.8	9.9
566	0.720	0.0752	0.992	1.043	0.980	2.9	1.3	4.2
565	0.894	0.0756	0.985	1.031	0.970	9.3	0.8	10.1

α_T FOR THE Kr-Xe SYSTEM AT 250 K

558	0.096	0.0188	0.985	1.055	0.986	5.7	0.8	6.5
559	0.292	0.0183	0.985	1.055	0.987	5.5	1.0	6.5
560	0.477	0.0194	0.985	1.054	0.986	4.2	0.8	5.0
562	0.700	0.0192	0.977	1.043	0.980	3.4	0.7	4.1
563	0.902	0.0204	0.978	1.043	0.980	4.7	0.9	5.6

[a]Mole fraction of lighter component.

[b](A) Correction from the exponential approach to equilibrium.
(B) Correction from the disturbance caused by pumping.
(C) Correction from back diffusion in the capillaries.
(D) Uncertainty from composition analysis.
(E) Uncertainty from temperature measurements.
(F) Total Uncertainty.

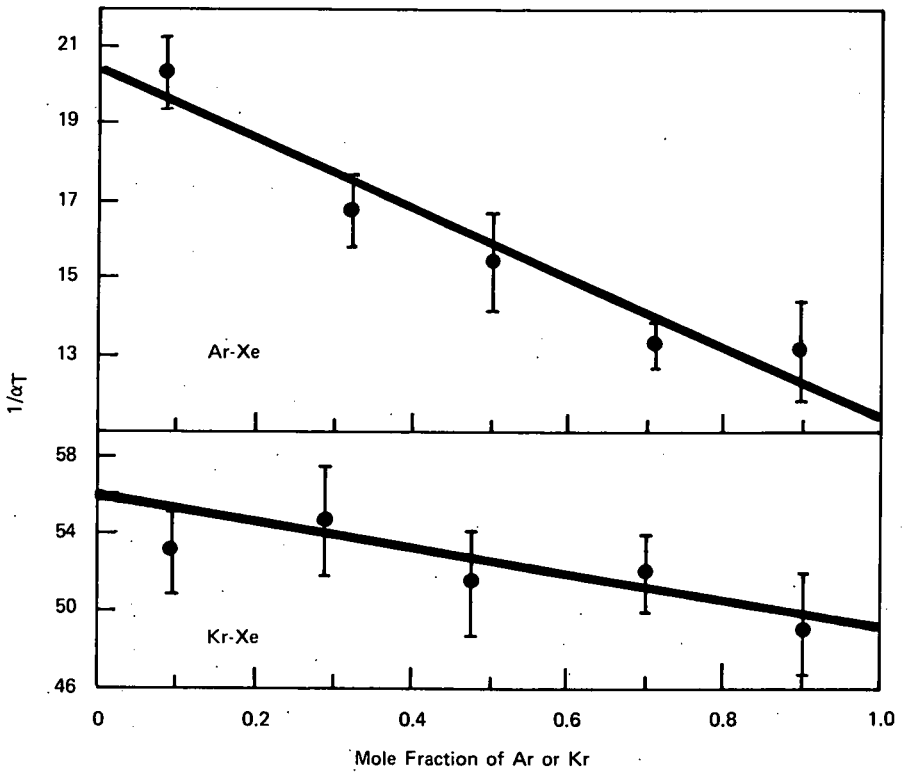

FIGURE 21 - Composition dependence of the thermal diffusion factor for Ar-Xe and Kr-Xe mixtures at an average temperature of 250 K. Estimated experimental uncertainties are shown as error bars. The solid line fits the data to a linear equation by least squares.

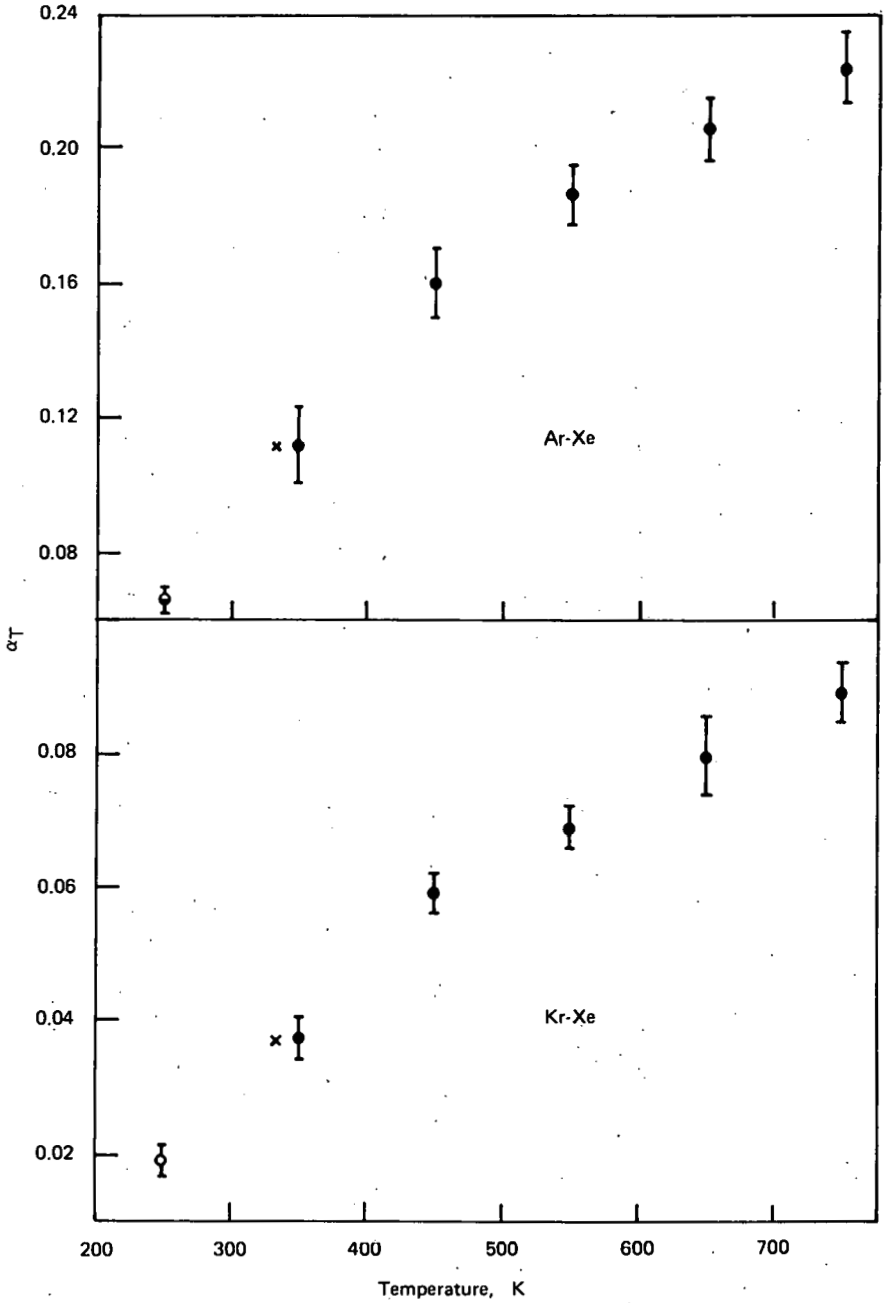

FIGURE 22 - Temperature dependence of the thermal diffusion factor for an equimolar mixture in the Ar-Xe or Kr-Xe system. The o was obtained from the least squares equation for $1/\alpha_T$; the X is the determination by Santamaria et al. (Reference 49).

References

1. Mound Laboratory Activities for the Division of Physical Research: January-June 1976, MLM-2354 (September 30, 1976), pp. 12-16.
2. W. K. Meckstroth and D. White, J. Chem. Phys., 34, 3723 (1971).
3. Mound Laboratory Activities for the Division of Physical Research: January-June 1976, MLM-2354 (September 30, 1976), pp. 22-25.
4. R. M. Cotts, Ber. Bunsenges, Physik. Chem., 76, 760 (1972).
5. A. J. Maeland, J. Phys. Chem., 68, 2197 (1964).
6. K. I. Hardcastle and T. R. P. Gibb, Jr., J. Phys. Chem., 76, 927 (1972).
7. H. Asano and M. Hirabayashi, Phys. Status Solidi A, 15, 267 (1973).
8. H. Asano and M. Hirabayashi, Phys. Status Solidi A, 16, 69 (1973).
9. D. G. Westlake, M. H. Mueller, and H. W. Knott, J. Appl. Cryst., 6, 206 (1973).
10. R. R. Arons, H. G. Bohn, and H. Lütgemeier, J. Phys. Chem. Solids, 35, 207 (1974).
11. H. Asano, Y. Abe, and M. Hirabayashi, Acta Metall., 24, 95 (1976).
12. B. Stalinski, Ber. Bunsenges, Physik. Chem., 76, 724 (1972).
13. J. Wanagel, S. L. Sass, and B. W. Batterman, Phys. Status Solidi A, 10, 49 (1972).
14. M. Engelsberg and R. E. Norberg, Phys. Rev., B5, 3395 (1972).
15. N. Boden and M. Gibb, Mol. Phys., 27, 1359 (1974).
16. D. G. Westlake, S. T. Ockers, M. H. Mueller, and K. D. Anderson, Metall. Trans., 3, 1709 (1972).
17. D. G. Westlake, S. T. Ockers, and W. R. Gray, Metall. Trans., 1, 1361 (1970).
18. Mound Laboratory Activities for the Division of Physical Research: January-June 1976, MLM-2354 (September 30, 1976), pp. 18-21.
19. A. Abragam and B. Bleaney, Electron Paramagnetic Resonance of Transition Ions, Clarendon Press, Oxford, 1970.
20. B. R. McGarvey, J. Phys. Chem., 71, 51 (1967).
21. W. Marshall, in Paramagnetic Resonance: Proceedings, Vol. 1, W. Low (ed.), Academic Press, New York, 1963, p. 347.
22. L. B. Lundberg, D. T. Cromer, and C. B. Magee, Inorg. Chem., 11, 400 (1972).
23. L. B. Lundberg, Structure and Bonding of Lithium-Rhodium Hydrides, PhD thesis, University of Denver (1968).
24. L. E. Murr, J. Less Common Metals, 34, 177-179 (1974).
25. Mound Laboratory Activities for the Division of Physical Research: July-December 1973, MLM-2118 (February 28, 1974), pp. 32-35.
26. Mound Laboratory Activities for the Division of Physical Research: January-June 1974, MLM-2168 (August 30, 1974), pp. 31-35.

27. Mound Laboratory Activities for the Division of Physical Research: January-June 1975, MLM-2241 (November 11, 1975), pp. 29-31.

28. Mound Laboratory Activities for the Division of Physical Research: July-December 1975, MLM-2296 (May 14, 1976), pp. 25-29.

29. Mound Laboratory Activities for the Division of Physical Research: January-June 1976, MLM-2354 (September 30, 1976), pp. 32-35.

30. Mound Laboratory Activities for the Division of Physical Research: July-December 1972, MLM-2013 (February 14, 1973), pp. 56-59.

31. Mound Laboratory Activities for the Division of Physical Research: January-June 1976, MLM-2354 (September 30, 1976), pp. 35-36.

32. Mound Laboratory Activities for the Division of Physical Research: July-December 1975, MLM-2296 (May 14, 1976), pp. 41-42.

33. Mound Laboratory Activities for the Division of Physical Research: January-June 1973, MLM-2068 (August 22, 1973), pp. 12-14.

34. Mound Laboratory Progress Report for August 1965, MLM-1287 (February 23, 1966), pp. 20-22.

35. Mound Laboratory Activities for the Division of Physical Research: January-June 1976, MLM-2354 (September 30, 1976), pp. 40-48.

36. W. L. Taylor, "Thermal Diffusion Factor for the ^{3}He-^{4}He System in the Quantum Region," J. Chem. Phys., 56, 834 (1973).

37. Mound Laboratory Activities for the Division of Physical Research: January-June 1974, MLM-2168 (August 30, 1974), pp. 15-19.

38. W. L. Taylor, "The Attractive Well in the Helium Interaction as Implied by Thermal Diffusion Experiments Between 2 and 5 K," in Low Temperature Physics - LT14, M. Krusius and M. Vuorio (ed.), Vol. 4, North-Holland Publishing Co., Amsterdam, 1975, pp. 433-436 (Proceedings of the 14th International Conference on Low Temperature Physics, Helsinki, Finland, 1975).

39. Stable Gaseous Isotope Separation and Purification: April-June 1969, MLM-1608 (November 15, 1969), p. 23.

40. Stable Gaseous Isotope Separation and Purification: January-March 1970, MLM-1728 (July 15, 1970), p. 28.

41. S. Weissman, "Thermal Diffusion Factors for ^{4}He-^{3}He at Low Temperatures," Phys. Fluids, 12, 2237 (1969).

42. H. K. Lonsdale and E. A. Mason, "Thermal Diffusion in Gases and the Approach to the Steady State," University of Maryland Report IMP-AEC-2, Part II, Appendix A, p. 119 (1957).

43. W. L. Taylor and J. M. Keller, "Transport Properties of Helium Using Beck's Potential," J. Chem. Phys., 54, 647 (1971).

44. J. M. Keller and W. L. Taylor, "Evaluation of Transport Properties of Gases: The Bruch-McGee Potential for Helium," J. Chem. Phys., 51, 4829 (1969).

45. Mound Laboratory Activities for the Division of Physical Research: July-December 1975, MLM-2296 (May 14, 1976), pp. 52-56.

46. Mound Laboratory Activities for the Division of Physical Research: July-December 1974, MLM-2198 (April 10, 1975), pp. 57-62.

47. Mound Laboratory Activities for the Division of Physical Research: July-December 1973, MLM-2118 (February 28, 1974), pp. 15-17.

48. Mound Laboratory Activities for the Division of Physical Research: January-June 1973, MLM-2068 (August 22, 1973), pp. 14-18.

49. C. M. Santamaria et al., J. Chem. Phys., 64, 1095 (1976).

Distribution

EXTERNAL

Technical Report Library, Monsanto, St. Louis
TID-4500, UC-4 and 22 (231)

J. A. Chacon, DAO
R. B. Craner, SLA
R. K. Flitcraft, MRC
W. J. Haubach, DPR
N. Haberman, DNRA
W. E. Moddeman
F. D. Stevenson, DPR
C. P. Sutter/R. N. Diebel, Atlantic Richfield
D. White
R. N. Zare

INTERNAL

V. L. Avona
R. C. Bowman, Jr.
W. T. Cave
R. J. DeSando
R. E. Eppley
C. W. Huntington
B. E. Jepson
L. V. Jones
C. M. Love
J. R. McClain
E. Michaels
W. J. Roos
W. M. Rutherford
R. A. Schwind
G. L. Silver
W. L. Taylor
H. L. Turner
R. E. Vallee
R. M. Watrous

Document Control
Library (15)
Publications (25)